QUARTERLY JOURNAL OF THE ROYAL METEOROLOGICAL SOCIETY
RMetS Royal Meteorological Society

High-resolution air-sea coupling impact on two heavy precipitation events in the Western Mediterranean

Journal:	*QJRMS*
Manuscript ID	QJ-16-0220.R2
Wiley - Manuscript type:	Research Article
Date Submitted by the Author:	n/a
Complete List of Authors:	Rainaud, Romain; CNRM UMR3589 LEBEAUPIN BROSSIER, Cindy; CNRM UMR3589 Ducrocq, Veronique; CNRM UMR3589 GIORDANI, Hervé; CNRM UMR3589
Keywords:	air-sea coupling, AROME, heavy precipitation events, HyMeX, mistral, NEMO

SCHOLARONE™
Manuscripts
For Review

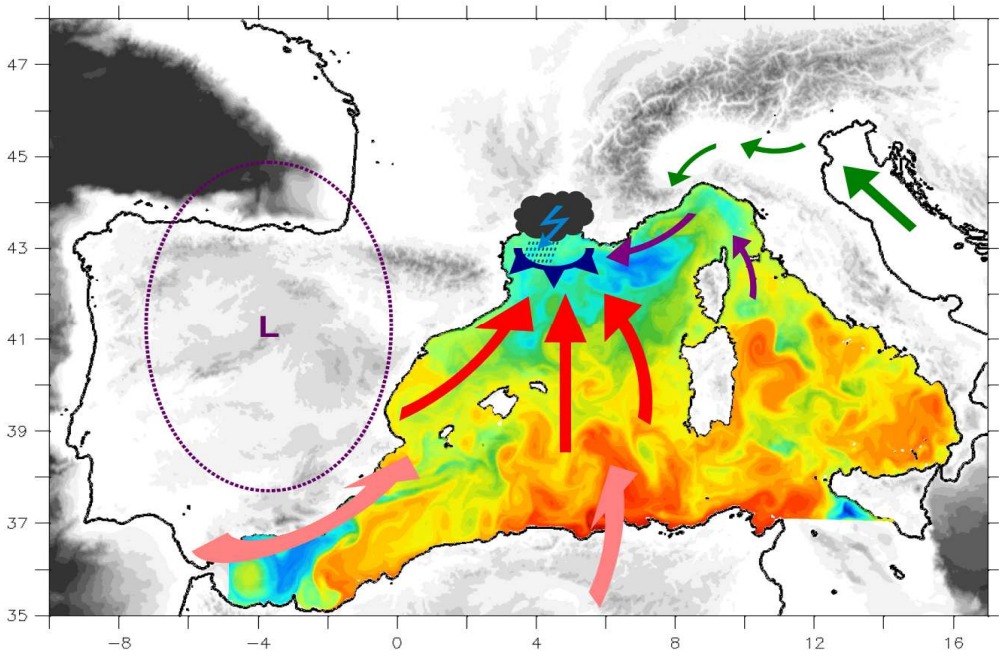
High-resolution air-sea coupling impact on two heavy precipitation events in the Western Mediterranean

R. Rainaud, C. Lebeaupin Brossier*, V. Ducrocq, H. Giordani

The AROME-NEMO WMED coupled model was developed to investigate the role of air-sea coupling on two heavy rainfall events.

For each case study, the coupled run is compared to two atmosphere-only AROME-WMED experiments with no SST evolution.

The large impact of the initial SST field on the precipitation forecast is re-asserted, and, the significant effect of the interactive 3D ocean coupling, with surface cooling notably due to entrainment, on the evaporation water supply for HPE is highlighted.



High-resolution air-sea coupling impact on two heavy precipitation events in the Western Mediterranean

R. Rainaud, C. Lebeaupin Brossier*, V. Ducrocq, H. Giordani

Centre National de Recherches Météorologiques (CNRM) UMR 3589 (Météo-France & CNRS), Toulouse, France

*Correspondence to: C. Lebeaupin Brossier, CNRM, 42 Avenue G. Coriolis, 31057 Toulouse cedex, France, cindy.lebeaupin-brossier@meteo.fr

For Peer Review

The Mediterranean Sea is an important source of heat and moisture for heavy precipitation events (HPEs). Moreover, the Ocean Mixed Layer (OML) evolves rapidly under such intense events. Whereas short-term Numerical Weather Prediction systems generally use low-resolution non-evolving Sea Surface Temperature (SST), the development of high-resolution high-frequency coupled system allows to fully take into account the fine-scale interactions between the low-level atmosphere and the OML which occur during HPEs.

The aim of this study is to investigate the impact of fine-scale air-sea interactions and coupled processes involved during the HPEs which occurred during the 12 to 15 October 2012 (IOP13) and 26 to 28 October 2012 (IOP16a/b) of the HyMeX first field campaign. For that purpose, the high-resolution coupled system AROME-NEMO WMED was developed. This system is based on the 2.5 km-resolution non-hydrostatic convection-permitting atmospheric model AROME-WMED and the 1/36°-resolution NEMO-WMED36 ocean model. The coupling frequency is 1h. To distinguish the effects due to the change in the initial SST field from that due to the interactive 3D ocean, the coupled run is compared to two AROME-WMED atmosphere-only experiments with no SST evolution during the 48-hour forecast cycles: one using the AROME-WMED SST analysis, the second using the SST field of the coupled experiment each day at 00UTC. The results of the three experiments re-assert that the SST initial condition strongly influences the HPE forecast, in terms of intensity and location. With water budget analyses, the significant impact of the ocean interactive evolution on the surface evaporation water supply for HPE is also highlighted. In case of strong and intense air-sea exchanges, like during the mistral event of IOP16b, the coupling reproduces the intense and rapid surface cooling and demonstrates the importance of representing the ocean turbulent mixing with entrainment at the OML base.

Key Words: air-sea coupling; AROME; heavy precipitation events; HyMeX; mistral; NEMO

Received . . .

© 2017 Royal Meteorological Society

1. Introduction

The Western Mediterranean coastal region is frequently affected by Heavy Precipitation Events (HPEs, accumulations >100 mm in 24 hours), mainly during fall, which sometimes lead to severe damages and human casualities. Over South-Eastern France, HPEs are generally generated by Mesoscale Convective Systems (MCSs) which develop eastward of an upper-level trough (Nuissier et al. 2008, 2011) and are favoured by a low-level moist unstable marine flow directed towards the mountainous coasts of the region (Fig. 1a). The lifting mechanisms leading to quasi-stationary MCSs generating the large rainfall amounts include orographic lifting, low-level wind convergence and cold pools due to precipitation evaporation (Ducrocq et al. 2008, 2016). The mountains and islands of the region induce deflection of the flow, channelling effects, lee cyclogenesis and blocking of the thunderstorm cold pools that act on the lifting mechanisms. These indirect effects of the terrain mainly result from the interaction of the large-scale flow with the orography of the region (Ricard et al. 2012). The moisture and velocity of the low-level flows, which influence the deflection of the flows by islands or mountains, making the environment more favourable to flow over/around depending on the Froude number, have been shown to have a significant role on the location of heavy precipitation (Bresson et al. 2012).

The Mediterranean area is also affected by strong regional winds, associated with low pressure systems over the region, channelled and accelerated in the steep valleys characteristic of the Mediterranean coastal area (Fig. 1b). In the North-Western Mediterranean area, the cold and dry regional winds known as mistral (northerly) and tramontane (north-westerly) frequently occur. Gusts exceeding 100 km h^{-1} are very frequent in South-Eastern France during such strong wind events and may cause substantial damages.

The Mediterranean Sea is a significant heat and moisture source (Duffourg and Ducrocq 2011) and air-sea exchanges play a key role during these intense events (Lebeaupin Brossier et al. 2008). These exchanges are expressed in terms of the turbulent fluxes of heat, moisture and momentum, which are controlled by gradients of temperature, humidity and velocity at the air-sea interface. The sea surface conditions and mainly the temperature (SST) thus control the exchanges between ocean and the atmosphere, together with the winds which modulate the efficiency of the exchanges. These interactions modify the low-level atmosphere stability and can notably impact the intensity of atmospheric convection and precipitation (*e.g.* Homar et al. 2003; Xie et al. 2005). The SST can influence the structure and organization of precipitating systems (tropical cyclone-like, convective or frontal systems), their life cycle, severity, propagation speed, and track, as shown by several numerical studies considering the sensitivity of HPEs to SST in the Western and Central Mediterranean region (*e.g.* Pastor et al. 2001; Lebeaupin et al. 2006; Miglietta et al. 2011; Romero et al. 2015; Stocchi and Davolio 2016). Not only the SST value, but also the SST patterns are characteristics that have to be accounted for in HPE high-resolution modelling and forecast. In addition, during intense meteorological events in the Mediterranean, significant interactions between the Oceanic Mixed Layer (OML) and the low-level atmosphere can occur on short time scales of only several hours (Lebeaupin Brossier et al. 2014). Generally, the intense and rapid sea surface evolution which occurs at fine-scale is not taken into account in Numerical Weather Prediction systems. Most of the time, the ocean conditions are prescribed using only a low- to medium-resolution SST initial field which does not evolve during the forecast run, especially for short-range high-resolution numerical weather prediction.

Past studies investigated the effects of coupling an ocean model to high-resolution atmospheric models in the context of severe weather short-range forecast.

Lebeaupin Brossier et al. (2009) developed the coupled system between the Meso-NH atmospheric model (Lafore et al. 1998) and the Gaspar et al. (1990) 1D ocean model to evaluate the air-sea coupled effects for three case studies in South-Eastern France. This study showed that the Mediterranean Sea loses energy to feed the atmospheric convection. The OML cools and deepens under the low-level wind jet. The interactive coupling reduces the atmospheric and oceanic responses compared to uncoupled runs. However, their conclusions are limited because of the short duration (18-24 hours) and small domain (around the Gulf of Lion) of their simulations. Moreover, using a 1D ocean model

For Peer Review

© 2017 Royal Meteorological Society

leads to SST errors during intense events, mainly because it does not take into account the 3D ocean circulation regulating the OML evolution (Davolio et al. 2015).

Pullen et al. (2006, 2007) showed that, in the Adriatic area, the 3D high-resolution (4 km) air-sea coupling, with the COAMPS (Coupled Ocean-Atmosphere Mesoscale Prediction System) model, improves the simulation of both ocean surface and low-level atmosphere during strong wind events. The ocean cooling under strong wind stabilizes the atmospheric boundary layer and reduces the heat exchanges and low-level wind. The same results were found by Small et al. (2011, 2012) in the Ligurian Sea during mistral events. The COAWST (Coupled Ocean-Atmosphere-Wave-Sediment-Transport Warner et al. 2010) coupled system was used at high resolution (up to 1 km-resolution for the atmosphere and up to 250 m-resolution for the ocean [and wave] model[s]) for several intense weather events over the Mediterranean region (Renault et al. 2012; Ricchi et al. 2016; Grifoll et al. 2016). These studies highlighted that the fully atmosphere-ocean[-waves] coupling improves the simulation results mainly in terms of surface heat fluxes, but also in terms of low-level atmosphere circulation and stability and on storm intensification.

The present study aims also at better understanding and evaluating the ocean-atmosphere coupling impacts but on HPEs and in the context of short-range and high-resolution weather forecasts.

The international HyMeX (*Hydrological cycle in Mediterranean Experiment*, www.hymex.org) program (Drobinski et al. 2014) investigates the Mediterranean hydrological cycle. A large part of the program is devoted to increasing the knowledge and the prediction skill of high-impact weather events in the area. Two field campaigns, called Special Observation Periods (SOPs), were organised in autumn 2012 and winter 2013 to document intense meteorological events and their environment.

During the first SOP (SOP1, between 5 September to 6 November 2012) focusing on heavy precipitation and flash-flood events, more than 200 instruments were deployed on land, in the air and at sea over the Western Mediterranean area (Ducrocq et al. 2014). Some of these instruments were devoted to measuring air-sea exchanges and marine atmospheric and oceanic boundary layers upstream of HPEs (*e.g.* gliders, moored and drifting buoys, CTD profiles, balloons and radio-soundings). Facilities like aircraft or ships were also used during the Intense Observation Periods (IOPs). Forecasts were used during the field campaign to support the instrument deployment in real-time. In particular, the Météo-France non-hydrostatic convective-scale atmospheric model AROME (Seity et al. 2011) was run in a dedicated version named AROME-WMED (Fourrié et al. 2015), producing each day 48 hours of forecast from 00UTC. A complete evaluation of the air-sea conditions in the AROME-WMED forecasts during SOP1 was done in a previous study (Rainaud et al. 2016). It showed that AROME-WMED forecasts fit very well with the meteorological observations over sea. However, significant biases (up to 4°C for the 2 m-temperature) were found very locally in the Gulf of Lion during a severe mistral/tramontane wind event (28 October 2012). Two possible sources of errors were identified: i) an overestimation of the sensible heat flux for such conditions by the turbulent fluxes bulk parameterization and ii) the fact that the SST does not evolve during the 48h-forecast, remaining as the initial analysis. This paper aims to address this latter issue by evaluating the impact of an evolving SST during the forecast, through a high-resolution 3D ocean-atmosphere coupling with the AROME-NEMO WMED system, on the representation of the air-sea interface processes and of two HPEs that occurred during SOP1.

The paper is organized as follows. The section 2 presents the numerical ocean-atmosphere coupled system and the experiments. The section 3 describes the two case studies. The impact of the coupling on the air-sea interface is shown in section 4, then in section 5, we describe the impact on the intense meteorological event forecast. Finally, the conclusions and perspectives of this work are given in the section 6.

2. Models and experiments

2.1. *The AROME-NEMO WMED coupled system*

The coupled system AROME-NEMO WMED combines the AROME atmospheric model (Seity et al. 2011) and the NEMO ocean model (Madec et al. 2008). The coupling interface includes SURFEX (Masson et al. 2013) and OASIS3-MCT (Valcke 2013).

For Peer Review

© 2017 Royal Meteorological Society

2.1.1. *The atmospheric model*

The atmospheric model, AROME-WMED (Fourrié et al. 2015) is the HyMeX dedicated version of AROME. It ran in real-time during the HyMeX SOP1 field campaign, producing each day a 48-hour forecast from the 00UTC AROME analysis. AROME-WMED covers a large domain over the Western Mediterranean area, from Portugal to Sicily and from the Atlas mountains to Northern Alps (Fig. 2). This model is non-hydrostatic and has a 2.5 km-horizontal resolution with 60 stretched η-vertical levels extending from near the surface (almost 10 m) to the top of the troposphere (around 1 hPa). The advection scheme is semi-lagrangian and the temporal scheme is semi-implicit. The boundary conditions are provided by the hourly forecast from the Météo-France global model, ARPEGE (Action de Recherche Petite Echelle Grande Echelle, Courtier et al. 1991). The turbulent scheme is the Cuxart et al. (2000) 1.5 TKE scheme used only for the vertical turbulence. Because AROME is a non-hydrostatic model and thanks to its horizontal resolution, the deep convection is explicitly solved, while the shallow convection is parameterized with EDKF (Eddy Diffusion Kain Fritsch, Kain and Fritsch 1990). The evolution of the five hydrometeor species (rain, snow, graupel, cloud ice and cloud liquid vapor) is given by the ICE3 scheme (Pinty and Jabouille 1998). The surface scheme in AROME-WMED is SURFEX (Masson et al. 2013). Each grid mesh is split into four tiles: land, towns, sea, and inland waters (lakes and rivers). Output fluxes are weight averaged inside each grid box according to the fraction of each respective tile, before being provided to the atmospheric model. The Interactions between Soil, Biosphere, and Atmosphere (ISBA) parameterization (Noilhan and Planton 1989) is activated over land tiles, whereas the Town Energy Budget (TEB) scheme is used for urban tiles (Masson 2000). Concerning inland waters, the Charnock (1955)'s formulation is used. Based on Rainaud et al. (2016)'s results, the sea surface turbulent fluxes bulk parameterization used is COARE 3.0 (Fairall et al. 2003) in this study. Radiative fluxes are computed with the Fouquart and Bonnel (1980) scheme (shortwave) and RRTM (Rapid Radiative Transfer Model, Mlawer et al. 1997) scheme (longwave).

2.1.2. *The ocean model*

The ocean model, NEMO-WMED36 (Lebeaupin Brossier et al. 2014), is a regional version of NEMO over the Western Mediterranean Sea (Fig. 2) with a horizontal resolution of 1/36° over an ORCA grid and with 50 z-stretched vertical levels with a 1-m thick first level. The domain has two open boundaries: one west at 4.8°W (60 km east of Gibraltar Strait) and one south at 37°N across the Sicily Channel. The Strait of Messina between Sicily and continental Italy is closed. The open boundary conditions come from the PSY2V4R4 daily analyses of Mercator-Océan, smoothed with a monthly averaging to avoid abrupt incoming flows. The PSY2 operational system (Lellouche et al. 2013) has a 1/12° horizontal resolution and covers the North-Eastern Atlantic Ocean, the North and Baltic Seas and the Mediterranean Sea.

In NEMO-WMED36, the tracer advection is computed using a TVD scheme (Barnier et al. 2006) to conserve energy and enstrophy. The turbulence closure scheme is the Blanke and Delecluse (1993) 1.5 TKE scheme, and in case of instabilities, the diffusivity coefficient is fixed at 10 m^2 s^{-1} (Lazar et al. 1999) to parameterize ocean deep convection. The sea surface height (SSH) is given by the filtered free surface scheme of Roulet and Madec (2000) and permits to keep a sea volume constant. The bottom friction follows a quadratic function with a coefficient which depends on the 2D mean tidal energy (Lyard et al. 2006). The runoffs are applied on the surface of the river mouths and come from the Beuvier et al. (2010) climatology.

2.1.3. *The air-sea coupling interface*

The coupled system AROME-NEMO is implemented using the SURFEX-OASIS coupling interface (Voldoire et al. 2017). This interface permits the field exchanges between the atmospheric and ocean models (Fig. 2). NEMO provides to OASIS the mean SST and horizontal surface current components (u_s and v_s) at the coupling frequency of one hour. These fields, after interpolation onto the AROME (SURFEX) grid, are used to compute surface fluxes at each subsequent atmospheric time step. The air-sea fluxes at the interface - namely the solar heat flux Q_{sol}, the net heat flux Q_{net}, the two components of the horizontal wind stress τ_u and

For Peer Review

© 2017 Royal Meteorological Society

τ_v and the atmospheric freshwater flux EMP - are computed by SURFEX and provided to OASIS, which then averages them over one hour, interpolates and sends them to NEMO at the coupling frequency.

The air-sea fluxes are computed taking into account near surface atmospheric and oceanic parameters, following the radiative schemes and turbulent fluxes parameterization:

$$Q_{sol} = (1-\alpha)SW_{down} \quad (1)$$

$$Q_{net} = Q_{sol} + LW_{down} - \epsilon\sigma SST^4 - H - LE \quad (2)$$

where SW_{down} and LW_{down} are the incoming components of the solar and infrared radiations, respectively. α is the albedo, ϵ is the emissivity and σ is the Stefan-Boltzman constant. Turbulent heat fluxes (H for sensible and LE for latent) are calculated with the COARE 3.0 parameterization (as suggested by Rainaud et al. (2016)'s results) and depend on the wind speed and on the air-sea gradients of temperature and humidity, respectively. The atmospheric freshwater flux is given by:

$$EMP = E - P_l - P_s \quad (3)$$

where E is the evaporation, corresponding to $E = LE/\mathcal{L}_v$ with $\mathcal{L}_v$ the vaporization heat constant. P_l and P_s are the liquid and solid surface precipitation rates (given by AROME-WMED).

The wind stress takes into account the ocean surface current (given by NEMO-WMED36):

$$\vec{\tau} = (\tau_u, \tau_v) = \rho_a C_D (U_s - U_a)(\overrightarrow{U_s} - \overrightarrow{U_a}) \quad (4)$$

with ρ_a the air density, C_D the drag coefficient given by the turbulent fluxes parameterization, $\overrightarrow{U_a} = (u_a, v_a)$ the wind at the lowest atmospheric model level (almost 10 m here) and $\overrightarrow{U_s} = (u_s, v_s)$ the ocean surface current.

The AROME-WMED domain is more extended than the NEMO-WMED36 domain west of the Gibraltar Strait and south of the Sicily Channel (Fig. 2). In addition, the Atlantic Ocean and the Adriatic Sea are not represented in NEMO-WMED36. So, in these areas, there is no air-sea coupling: the SST comes from the AROME-WMED initial analysis and is constant during the run, and, horizontal current is considered null.

2.2. *Sensitivity experiments*

To evaluate the impact of the air-sea coupling on the forecast of severe weather events, three sensitivity experiments have been performed for two case studies (see section 3).

The reference experiment (called ARCO) is an atmosphere-only AROME-WMED experiment. In ARCO, the initial conditions come from the AROME-WMED analysis, in particular the analysed SST, which is built by combining a 2D optimal interpolation of in-situ data with the CANARI system (Taillefer 2002) and the OSTIA (Donlon et al. 2012) product (see Rainaud et al. 2016, for more details on the AROME-WMED SST analysis). In ARCO, the SST field is kept constant during the forecast cycle.

The CPLOA experiment is the ocean-atmosphere coupled run using AROME-NEMO WMED. The atmospheric initial conditions come from the AROME-WMED analysis. For every 4-day case study, 48-hour forecasts are issued each day from the 00UTC analysis. The first day, the ocean is initialized from the outputs of a free (without any data assimilation) NEMO-WMED36 simulation (Rainaud 2015). This free ocean simulation was itself initialized on 5 September 2012 (at the beginning of HyMeX SOP1) by the Mercator Océan PSY2V4R4 analysis and driven by air-sea fluxes obtained from the AROME-WMED forecasts (Rainaud et al. 2016). For the following forecast production cycles, the ocean conditions at 00UTC (day D) are provided by the CPLOA 24-hour [ocean] forecast based on the day before (D-1; range +24h). The scheme in Figure 3 summarizes the protocol of the CPLOA experiment. From an atmospheric point-of-view, CPLOA is similar to ARCO except the initial SST field and that the SST evolves interactively during the forecast.

The third experiment (called SSTHR) is also an atmosphere-only AROME-WMED experiment, but it uses the SST issued from CPLOA at 00UTC each day and keeps it constant during the 48h-forecast. This experiment permits to distinguish the impact of the modification of the initial SST field (ARCO versus SSTHR) from the impact of the interactive SST evolution allowed by the coupling (SSTHR versus CPLOA). As the ocean initial state is taken from a free-running ocean simulations without data

For Peer Review

© 2017 Royal Meteorological Society

assimilation of oceanic observations in CPLOA and SSTHR, the SST field of these experiments are expected to have greater biases with respect to the observations than the AROME analysis used in ARCO, but with finer and more realistic patterns. While some comparisons against observations are provided in the following, their objective is mainly to support the evaluation of the differences between the simulations rather than as an objective measure of the benefit of ocean-atmosphere coupling for high-resolution NWP systems (in which data assimilation should be used to produce the initial ocean state).

3. Case studies

Two case studies have been chosen from the HyMeX SOP1 period because they include the two kinds of intense weather events of interest: first a moderate mistral episode followed by an HPE during the Intense Observation Period 13 (IOP13, Rainaud et al. (2016)), and secondly, an HPE followed by a severe mistral event during IOP16a/b (Ducrocq et al. 2014; Duffourg et al. 2016). Moreover, for these two IOPs, air-sea exchanges have been suggested playing a significant role (Rainaud et al. 2016; Thévenot et al. 2016). A brief description of the events is given in the following.

3.1. IOP13: Moderate mistral followed by HPE

The IOP13 took place between 12 and 15 October 2012. According to Rainaud et al. (2016), the event has been split in three phases following the wind regime. The first phase, from 12 October at 01UTC to 13 October at 10UTC, was characterized by high surface pressure over Catalonia and low surface pressure over Liguria inducing mistral and tramontane over the Gulf of Lion. During this first phase, convective precipitation occurred in the Catalonian sub-basin and Balearic Islands. The second phase took place between 13 October 11UTC and 14 October 03UTC and was characterized by a low wind regime in the Gulf of Lion and no precipitation. Finally, the third phase, from 14 October 04UTC to 15 October 00UTC, was characterized by a low-level south-westerly flow (Fig. 4a), associated with a surface low over Spain. The mechanisms involved in the MCS development over South-Eastern France during IOP13 are described in Duffourg et al. (2017, rev) and in a lesser extent in Barthlott and Davolio (2016) and Rainaud et al. (2016). The MCS that formed over South-Eastern France was fed by a marine moist southwesterly low-level jet topped with a drier layer and extremely dry air above 2500m ASL. The first convective cells developed around midday on 14 October 2012 over the first foothills facing the moist and conditionally unstable low-level flow advected from the Sea. According to Duffourg et al. (2017, rev) using a realistic 2.5km-resolution simulation, downstream of the upward motions, evaporative cooling under the precipitating cells appeared. This initiated a backbuilding process with new convective cells forming upstream while the older cells were transported northeastward by the mid-to-upper level southwesterly winds. The cold air formed by evaporative cooling under the precipitating cells progressively filled the valleys and then spread out over the plains upstream of the coastal orography, blocking the inland advection of the marine moist low-level flow. After 15UTC, the main convective ascents were located not only on the coastal mountainsides but also on the leading edge of the cold air pool. The cold pool thus played a major role in shifting the location of the precipitation from the bottom of the valleys to the coasts and over the sea. The most intense convection and heavy precipitation in the French Azur Riviera and Italy (Gulf of Genoa) occurred between 14 October 16UTC and 15 October 00UTC. Up to 120 mm in 24h were recorded in the Liguria region (Fig. 5a). During this event, a tornado was also observed near Marseille (Ducrocq et al. 2014).

For this case, the three experiments start on 11 till 14 October 2012.

3.2. IOP16a/b: HPE followed by a severe mistral event

The second case study, between 26 and 29 October 2012, is composed of two IOPs: IOP16a the 26 October and IOP16b the 27-28 October.

The study of Duffourg et al. (2016) details the mechanisms acting during IOP16a. On the early morning of 26 October, moist and conditionally unstable air was carried by a south-easterly low-level jet over the Gulf of Lion where a MCS formed and then split in two separate systems. One of the MCS (MCS1a) progressed northwards from 06UTC then decaying over the Cévennes (Massif Central). The other one (MCS1b) progressed northeastwards over the Mediterranean Sea and reached the southeastern France coasts

For Peer Review

(Var region) where it induced up to 150 mm in 24h (Fig. 5b), some local floods and 2 casualties in Toulon. The major initiation and maintenance mechanism was the convergence of the south-easterly low-level jet with the south-westerly flow along the Spanish coasts, associated with a secondary low pressure anomaly that formed in the lee of the Iberian mountains, as highlighted by Duffourg et al. (2016). As this surface low progressed eastwards and deepened, the convergence line intensified. Near surface cooling appeared below the MCS that perturbed the low-level flow and intensified the low-level convergence. A third MCS called MCS2 formed on the Gulf of Genoa and affected the Italian coasts, inducing up to 250 mm in 24h (Fig. 5b). In this paper, only the impact on forecast of MCS1a and MCS1b is examined.

The next day, the low reached the Gulf of Genoa, where it stayed till the end of 28 October. Associated with a very cold air break at high levels, it induced a severe mistral from the south of France and the Gulf of Lion to Corsica, Tunisia and the Tyrrhenian Sea. This severe wind event induced 2 fatalities in France. High waves (significant height up to 6.5 m at the LION buoy) were observed from Catalonia, Balearic Islands, France to Italy inducing damages. Finally, this mistral episode produced a drastic change of the whole Western Mediterranean Sea in terms of stratification, with a very rapid and intense cooling and a large mixing, as evidenced by Lebeaupin Brossier et al. (2014).

For this case, our sensitivity experiments start on 25 till 28 October 2012.

4. Effects on the air-sea interface

4.1. Sea Surface Temperature

The air-sea coupling impact is first examined on the SST field, after 48h of simulation.

For 13 October 00UTC, the CPLOA and SSTHR SST field present finer scale structures than in ARCO (Fig. 6a,d,g). The ARCO SST is slightly higher ($\leq$0.5°C) than the CPLOA SST after 48h forecast, on average over the entire domain. The largest differences are found in the Alboran Sea, the southern Tyrrhennian Sea and around the Balearic Islands (Fig. 6m). Locally, the SST in ARCO is lower, notably in the Gulf of Lion and along the Algerian coasts. These discrepancies come mainly from the different initial SST field rather than from the SST evolution during the forecast run, as the differences between ARCO and SSTHR (Fig. 6j) are larger than between SSTHR and CPLOA (Fig. 6p). The cooling induced by mistral during the phase 1 of IOP13 and simulated by CPLOA is small (Fig. 6d).

For IOP16a (27 October 00UTC), the SST in ARCO is lower than in CPLOA in the Gulf of Lion but higher in the south of the domain (Fig. 6b,e,n). The SST differences between ARCO and CPLOA arise mainly from the differences in the initial conditions (Fig. 6k,n,q). Indeed, the ocean surface evolution in 48h is small in CPLOA (if compared to SSTHR, Fig. 6e,h,q). Locally, large differences in term of gradient are found between ARCO and CPLOA. For example, between the Gulf of Lion and the Balearic Islands, the SST meridian gradient is $\sim 1°C$ in $\simeq$100 km in CPLOA while it is around 3°C in $\sim$100 km in ARCO. At the same time, the zonal gradient in the Ligurian Sea is more pronounced in CPLOA than in ARCO.

Looking at the 48h forecast for 29 October 00UTC (IOP16b), the coupled SST is significantly lower than the ARCO SST (almost 2°C over the basin, Fig. 6c,f,o) while the ARCO and SSTHR SST are relatively similar in terms of mean values (Fig. 6f,i,l). This shows the major evolution of the OML during the two days of IOP16b (Fig. 6r), which is not taken into account in the uncoupled forecast. This strong ocean cooling is more stamped in the Gulf of Lion (Fig. 6r) and is equitably distributed along the two days. It is due to two different mechanisms, as highlighted in Lebeaupin Brossier et al. (2014): First, dry and cold air transported by mistral leads to strong air-sea gradient of temperature and humidity at the sea surface, so to strong turbulent fluxes corresponding to extraction of heat and moisture from the OML to the low-level troposphere. Secondly, the strong wind induced a large turbulent mixing in the ocean, so, a deepening of the OML, which entrains colder water from below the ocean thermocline.

To sum-up, the large differences in SST between the uncoupled and coupled runs are due to the presence of fine structures in CPLOA (and SSTHR). Indeed, the NEMO-WMED36 ocean model produces numerous mesoscale eddies and fronts in the Western Mediterranean basin and well reproduces the dynamics and main patterns of the surface circulation described by Millot

For Peer Review

© 2017 Royal Meteorological Society

(1999), *i.e.* the anticyclonic gyre in the Alboran Sea, the Algerian current and coastal eddies, the Northern Current and the Balearic front. On the contrary, the AROME SST analysis used in ARCO exhibits a smooth north-south gradient. Even though the daily OSTIA SST product is refreshed by the assimilation of 3-hourly observations for the AROME SST analysis, the in-situ data are too few to permit to describe these fine-scale structures. Nevertheless, the AROME-WMED SST analysis (used in ARCO) is updated every day with observations unlike the simulated SST of NEMO-WMED36 (used as initial conditions for SSTHR and evolving in CPLOA). The comparison between SSTHR and CPLOA shows that the interactive coupling may produce very large differences up to 5°C after only 48h due both to large surface forcing and ocean turbulent mixing.

4.2. *Turbulent fluxes*

The impact of the coupling on turbulent fluxes is evaluated when the strong low-level wind is established over sea for IOP13 phase 3 (14 October 18UT), IOP16a (26 October 12UT) and IOP16b (28 October 00UT). In the following, we consider separately the *short-range* forecast (hereafter SR) as the forecast from +1h to +24h and the *long-range* forecast (hereafter LR) from +25h to +48h. Figure 7 compares the hourly total turbulent heat flux, which is the sum $-(H + LE)$ and is negative for an ocean [atmospheric] heat loss [gain].

For the two HPE situations, *i.e.* IOP13 phase 3 and IOP16a, the total heat flux is between -50 and -250 W m^{-2} in the reference experiment ARCO. Larger [in absolute value] heat losses up to -500 W m^{-2} are found near the Balearic Islands, where there is a maximum in the south-westerly low-level wind intensity (Fig. 7). For IOP13, another maximum of heat loss (-500 W m^{-2}) is found near the coasts of the Gulf of Lion associated with a new onset of a mistral spell. Considering SR, in CPLOA and SSTHR, the heat loss is slightly lower (by only ∼4 W m^{-2} on average) than in ARCO (Fig. 7). The SST fine scale structures in CPLOA and SSTHR induce local differences in the temperature and humidity air-sea gradients which lead to significant local differences in the flux fields (±200 W m^{-2}) with respect to ARCO ones, in particular near the Balearic Islands and in the Gulf of Lion, where the wind is the most intense. The simulated ocean evolution is small during these two HPEs. As a consequence the flux differences are small between CPLOA and SSTHR (for SR and LR, not shown). The differences between CPLOA-LR and CPLOA-SR (not shown) are similar to the differences between ARCO-LR and ARCO-SR, *i.e.* mostly due to differences in the atmospheric forecast.

For IOP16b, corresponding to the strong mistral spell, the total turbulent heat loss affects a wide part of the Western Mediterranean Sea and is very high [in absolute value], up to -1500 W m^{-2} in the Gulf of Lion (Fig. 7). For SR forecasts, the heat loss in CPLOA is globally lower (by 20 W m^{-2}) than in ARCO. Even if there are turbulent flux differences due to initial SST conditions as estimated by comparing ARCO to SSTHR, there is a significant part (50% on average) of the differences between CPLOA and ARCO which is due to the ocean evolution. Indeed, the ocean cooling due to mistral reduces the air-sea temperature gradient, itself inducing a decreasing of the heat loss. The impact of the interactive ocean is more significant (difference up to 500 W m^{-2}) for LR forecasts because of a longer drift from the ocean initial state corresponding to the large cooling of 5°C in 48h in the Gulf of Lion in that case (as shown in Fig. 6f,i).

5. Impacts on intense weather event forecast

5.1. *Heavy precipitation*

The impact of the air-sea coupling is investigated here for heavy precipitation during the IOP13 phase 3 and IOP16a. In the following, if the ARCO experiment serves as a reference, as it is the state-of-the-art of the current high-resolution NWP system, the role of the air-sea coupling on the forecast is only shown when comparing CPLOA with SSTHR.

5.1.1. *Rainfall amounts*

For all the SR experiments of IOP13 phase 3, the location of precipitation over South-Eastern France is overall in agreement with rain-gauge observations (Figs. 5a and 8), even if, the heaviest precipitation in ARCO-SR experiment occur around Nice whereas it is more extended from Nice to Genoa in CPLOA-SR and SSTHR-SR experiments (Fig. 8). BIAS, RMSE and correlation coefficients have been computed for the 24-h accumulated rainfall

For Peer Review

© 2017 Royal Meteorological Society

amounts for the three simulations against observations (Tab. 1). In addition, categorical scores considering different thresholds of daily accumulated rainfall amount were also computed (see the Appendix for definition). Figure 9 shows the POD, FBIAS and ETS scores. These scores show globally that ARCO is closer to the observations than SSTHR. The discrepancies between the experiments appear only for higher thresholds ($<$ 10 mm in 24 h). A SST evolving during the forecast run improves the scores (CPLOA to compare to SSTHR). For the LR experiments, the precipitating system is located further inland, in comparison with observations. The scores against rain-gauge data confirm weaker performances of the longer range experiments than the shorter range ones (Tab. 1 and Fig. 9). In addition, the differences between the LR experiments are weaker, even though ARCO is still the closest to the observations. No difference is clearly found in the mesoscale environment and the mechanisms involved in heavy precipitation during IOP13 *(see Fig. S1 in the supporting information file)*. The differences in precipitation seem rather due to small differences in the moisture contribution of the Western Mediterranean Sea throughout the simulation integration, which slightly modify the instability of the marine low-level flow. This point is examined with water budgets in the following section.

For the IOP16a, all the SR forecasts simulate rainfall amounts over the Cévennes linked to MCS1a larger than observed (Figs. 5b and 10). The simulations show more differences between them for MCS1b, with the best representation of rainfall amounts over the Var region for CPLOA-SR (Figs. 5b and 10). The scores against the 24h-cumulated rainfall observations indicate overall weak performances for the three experiments (Tab. 2, Fig. 11). This is also the case for the LR experiments. Any experiment performs better than the others as the ranking varies from one score to an other. Larger differences between experiments are found for the LR forecasts (Fig. 10) when comparing the heavy precipitation associated with MCS1a and MCS1b. CPLOA-LR underestimates intense rainfall associated with MCS1b and represents too intense rainfall for MCS1a. On the contrary, ARCO-LR simulates a more intense MCS1b. Finally, SSTHR-LR is between the two other experiments and represents intense rainfall for the two MCS.

The mechanisms involved in the formation and evolution of MCSs (Duffourg et al. 2016) are the same for the three experiments. Locally differences in the mesoscale environment simulated by the three SR or LR experiments are perceptible *(see Fig. S2 and S3 in the supporting information file)*. As example, for LR forecasts, instability and moisture are lower in the south-westerly low-level flow (around the Balearic Islands) in CPLOA-LR and SSTHR-LR compared to ARCO-LR. This can be related to a lower SST and to lower heat fluxes in this area. However, as the largest contributing area of moisture is located in the south-easterly flow (West of Sardinia), these differences lead to small impacts on the convection intensity. The secondary surface low which forms in the lee of the Pyrenees deepens more in SSTHR-LR than in CPLOA-LR, itself more than in ARCO-LR. The air cooling in the same area is also less intense in SSTHR-LR than in CPLOA-LR, itself less than in ARCO-LR. Indeed, the SST and the heat fluxes are lower in this area in ARCO-LR than in CPLOA-LR/SSTHR-LR at the beginning of the simulation. During the CPLOA simulation, SST progressively slightly decreases, and so do the surface heat fluxes in absolute value. These differences in terms of surface heat fluxes directly affect the low-level atmosphere stability and then the cyclonic circulation at low-level and thus it slightly modifies the convergence in the Gulf of Lion and the convection organization. CPLOA-LR underestimates intense rainfall associated with MCS1b and represents too intense rainfall for MCS1a. On the contrary, ARCO-LR simulates a more intense MCS1b. Finally, SSTHR-LR is between the two other experiments and represents intense rainfall for the two MCSs.

5.1.2. *Water budgets*

In order to analyze how much the water vapour amount within the atmospheric boundary layer is different, and thus the water supply available for heavy precipitation systems, total water content budgets are computed over a 3D box over the North-Western Mediterranean. The water budget computation follows Duffourg and Ducrocq (2013), with the time variation of the total atmospheric water (vapour and hydrometeors) storage S given by:

$$\Delta S = E - P + (Qn + Qe + Qs + Qw) + r \qquad (5)$$

where E is surface evaporation and P precipitation in surface (corresponding to atmospheric water losses for the box). Qn, Qe,

For Peer Review

Qs and Qw are the vertically integrated horizontal water fluxes across the vertical sides of the box for the north, east, south and west faces, respectively. r is the sum of the vertical transport at the top of the box and of a residual term due to the offline computation of the different terms. r has been verified as negligible when the top of the box is the model highest layer, so, for a less thick layer, r is controlled by the vertical flow at the top of the box.

The water budget is evaluated for a 50 hPa-height (corresponding to nearly 500 m) box covering a wide part of the North-Western Mediterranean Sea (Fig. 12) in order to focus on the marine low-level flow feeding the convective systems. Figure 13a presents the budget terms during IOP13 phase 3 in CPLOA. The vertically integrated horizontal water fluxes reflect the low-level atmospheric circulation which mainly consists of a southerly to southeasterly flow, with thus water inputs from the south, then from the south-west, and outputs to the north and east. Precipitation is simulated in the evening (after 18UTC) in the box, thus corresponding to a water loss (Fig. 13a). As precipitation starts, r becomes larger in absolute value, with negative values between 16UT and 21UT related notably to an upward flux of water due to convection, then positive indicating a water gain, *i.e.* a downward flux on average through the top of the box. Evaporation from sea increases along the day from 45 to 80 mg m^{-2} s^{-1}, due to the enhancement of the low-level wind during the day. E represents a significant contribution to the total water supply, up to 40% of the water supply (Fig. 13a), mostly from the region between Catalonia and the Balearic Islands (Fig. 7). But, above all, the largest contribution comes from outside (south) of the box, possibly from the Algerian basin as suggested by Rainaud et al. (2016), and crosses the North-Western Mediterranean area to supply moisture to the precipitating system over South-Eastern France. Figure 13b allows to assess the impact of coupling on the evaporation from the Sea. It shows the surface evaporation E for the three experiments and for SR and LR forecasts. E is lower in CPLOA compared to ARCO, in agreement with the results found in section 4.2 and shown in Figure 7. E for SSTHR-SR and CPLOA-SR are close, whereas SSTHR-LR is intermediate in term of evaporation between ARCO-LR and CPLOA-LR (corresponding to -10% and +10% for E, respectively). In conclusion, for that case, the water budget shows a quite large effect of coupling on the surface evaporation. The relative impacts of the interactive ocean during the forecast run and of the different initial SST have been estimated for SR[LR] forecasts to be of about 25[50]% and 75[50]%, respectively. For IOP16a, the relative impacts are assessed to be 10[20]% for the interactive ocean and 80[90]% for the initial SST field *(see Fig. S4 in the supporting information file)*.

5.2. *Severe mistral*

Figure 14 shows the evolution of the wind speed, the 2 m-temperature and the SST at the LION buoy [4.7°E-42.1°N] during IOP16b (27-28 October 2012). It shows the large increase in the wind speed and the decrease in temperature associated with the mistral. All the experiments reproduce quite well this rapid evolution of the low-level atmosphere. At the end of 28 October (range +42 to +46h), as the wind starts decreasing, differences between the experiments are maximum. The 10 m-wind speed is lower by 0.8 m s^{-1} in SSTHR and by 1.5 m s^{-1} in CPLOA compared to ARCO. However, compared to the buoy observation, all the experiments overestimate the wind speed (by up to 5 m s^{-1} at range +30h). The largest differences in the 2 m-temperature between the experiments are also found on 28 October: up to +0.1°C for SSTHR and of -0.4°C for CPLOA compared to ARCO. In the coupled run, the cold front induced by the mistral goes a little more to the south than in ARCO (not shown). This is probably due to a cooler atmospheric boundary layer as an integrated effect of the lower SST and heat fluxes under mistral (Fig. 6c,f,i and 7) and also to the triggering of the frontal convection more in the south related to the position of the warm Algerian eddies in CPLOA (Fig. 6f).

As already highlighted, during this mistral event, the SST strongly decreases (Fig. 14). This decrease is only represented in the coupled experiment (-2.3°C in 48h against -4°C in 48h observed at the LION buoy). However, CPLOA presents initial and final biases in SST. In the morning of 27 October, the cold SST bias (-0.8°C) is associated with a too thin OML (20 m-depth against 30 m-depth according to temperature observation from the bathymetric thermistance chain at the LION buoy). This is due to errors in the initial ocean state issued from the free NEMO-WMED36 run started at the beginning of September and

For Peer Review

© 2017 Royal Meteorological Society

not refreshed by ocean data assimilation since then. The biases in SST and thermocline position at Lion are indeed already present before IOP13 and IOP16a *(see Fig. S5 and S6 in the supporting information file)*. On the afternoon of 28 October, CPLOA SST is overestimated (+0.9°C) although the Mixed Layer Depth (MLD) is around 50 m-depth as observed. In fact, this overestimation is explained by too warm waters located below the OML which make the cooling by entrainment at the bottom of OML not intense enough in CPLOA.

As also shown by Lebeaupin Brossier et al. (2014), the OML cooled and deepened drastically over the whole Western Mediterranean basin during IOP16b due to large surface heat loss and turbulent mixing. The coupled experiment presented here shows the important role of the OML during this severe mistral event with at the same time a downward heat transport below the thermocline to the deeper ocean layers by mixing/deepening, and, in surface a moderation of the sensible and latent heat fluxes in absolute value and of the evaporation. As a consequence, the 2m-air temperature (and 2m-specific humidity, not shown) is slightly lower in the CPLOA forecast (than in SSTHR, Fig. 14).

6. Conclusions and perspectives

This study presents the first application and validation of the high-resolution high-frequency air-sea coupled model AROME-NEMO WMED, considering the most frequent severe weather events of the Western Mediterranean region, *i.e.* HPEs and mistral. Using three sensitivity experiments, the impact of two different effects on the atmospheric forecast were considered: the change in the initial SST field and the impact of an interactive 3D ocean. This study aims at investigating the role of the air-sea coupling on the forecast with the comparison between CPLOA and SSTHR. If ARCO serves as a reference, it is important to point out that the coupled experiment design, with the use of free-running simulation to initialize the ocean model, prevents from a direct verification of the forecast skill.

For IOP13, corresponding to a moderate mistral episode followed by an HPE, the coupled interactive ocean induces a small decrease in the SST and in the surface heat fluxes. Nevertheless, the location of the heaviest precipitation is modified. An analysis of the water budget highlights that, despite a weak OML evolution during that case, coupling leads to a decrease in the Mediterranean Sea evaporation and water supply by up to ∼20% compared to the ARCO experiment, but more than a half is due to the change in the initial SST field. In addition, the two moisture extracting areas (*i.e.* the Catalonian Sea and the Algerian basin) suggested by Rainaud et al. (2016) were confirmed by this budget evaluation.

For IOP16a, a large sensitivity of the MCSs forecast was highlighted. In particular, the intensity of MCS1b over the Var region is completely modified with different sea surface conditions, for the benefit of MCS1a, which affects the Cévennes. In fact, the split of MCS1a in two MCSs which occurred over the Gulf of Lion seems to be very sensitive to the sea surface conditions and, furthermore, the MCS splitting there is a challenging process to correctly reproduce in numerical simulations of IOP16a. As for IOP13, the impact of the interactive ocean evolution is more important for long-range than for short-range forecast, because the OML cooling increases with the forecast range and modifies the intensity of the precipitating system.

The coupled experiment is able represent the intense and rapid OML cooling and deepening which occurred during the severe mistral event of IOP16b. It also confirms Lebeaupin Brossier et al. (2014) results, meaning that, in addition to the large surface heat loss, the entrainment of cold water at the OML base is an efficient process that significantly contributes to the sea surface cooling and, so, that is important to take into account. The OML deepening by entrainment which strongly contributes to the OML cooling by a downward heat transfer into the deeper oceanic layers and thus to the decrease in the surface turbulent heat fluxes towards the atmosphere, is thus a crucial coupled process. AROME-NEMO WMED was also recently applied for the study of dense water formation triggered by mistral and tramontane winds during HyMeX SOP2 (Lebeaupin Brossier et al. 2017), illustrating its benefit for the analysis of the fine-scale air-sea coupled processes.

Finally, the AROME-NEMO coupled system demonstrates that the air-sea interactive coupling affects the high-resolution atmospheric deterministic forecast. Nevertheless, additional sensitivity tests should be performed in order to better estimate the benefit of a ocean-atmosphere coupled systems for operational

For Peer Review

© 2017 Royal Meteorological Society

purpose. First, the obtained results only concern two HPEs and one mistral case. Further investigations must be undertaken for several other situations in order to assess the coupling impact. Secondly and as previously mentionned, in our coupled experiments, the ocean initial state arose from a free-running ocean simulation. The ocean state used as initial conditions is thus not as close from the real ocean state as the one that could be obtained through ocean data assimilation of the recent observations. The next step will be thus to use a high-resolution operational ocean analysis to initialize the ocean component of AROME-NEMO coupled system, as those provided by the *Copernicus Marine Environment Monitoring Service* (CMEMS). The step further towards operational real-time forecast would be to explore strategies for combining ocean data assimilation and atmosphere data assimilation for the AROME-NEMO system. Another perspective is to take into account the sea state with the introduction of a wave model in the coupled system, as it strongly impacts the sea surface turbulent fluxes and thus it can significantly modify the weather forecast (Renault et al. 2012; Ricchi et al. 2016; Thévenot et al. 2016; Bouin et al. 2017 rev.; Voldoire et al. 2017).

Acknowledgements

This work is a contribution to the HyMeX program (*HYdrological cycle in the Mediterranean EXperiment* - www.hymex.org) through INSU-MISTRALS support. The authors acknowledge the DGA (Direction Générale de l'Armement), a part of the French Ministry of Defense, for its contribution to Romain Rainaud's PhD. The authors thank Marie-Noëlle Bouin (CNRM) and the CMM team of Météo-France who manage and provide the observations of the LION moored buoy, Mercator Océan for supplying the PSY2V4R4 analysis and the HyMeX database teams (ESPRI/IPSL and SEDOO/OMP) for their help in accessing the data. The authors also thank Nadia Fourrié (CNRM) and the SWAPP system team (Météo-France) who helped us in the implementation of the AROME-WMED experiments and coupled simulations. Finally, the authors gratefully acknowledge Bertrand Decharme and Aurore Voldoire (CNRM) for their invaluable help in the SURFEX-OASIS coupling interface development.

The authors want to dedicate this work to the memory of Françoise Taillefer, who devoted much of her work to the improvement of the marine surface conditions in the Numerical Weather Prediction systems of Météo-France. Her enthusiasm and encouragements will be missing.

Appendix

Similarly to Ducrocq et al. (2002), the following skill scores were computed using a 2×2 contingency table (Tab. A) considering different thresholds of rainfall amounts:

- the frequency bias $FBIAS = (b+d)/(c+d)$;
- the probability of detection $POD = d/(c+d)$;
- the equitable threat score $ETS = (a-H)/(a+b+c-H)$;

with $H = [(a+b)(a+c)]/(a+b+c+d)$ referring to the expected number of correct simulated values below the threshold with a random simulation. The FBIAS measures the ability of the model to forecast the occurrence of the event over the threshold. The POD describes the ability in representing the size of the event. The ETS score measures the ability to reproduce the event taking into account its location.

A perfect forecast has FBIAS, POD and ETS equal to 1.

Supporting information

The following supporting information is available as part of the manuscript:

Figure S1. IOP13, 14 Oct 2012 16UT: [*top panels*] Radar reflectivities (colors, in mm h^{-1} equivalent), Integrated Water Vapor over 28 kg m^{-2} (grey area), wind at 950hPa (arrows, m s^{-1}) and CAPE over 750 J kg^{-1} (red contour), and, [*bottom panels*] θ'_w at 925 hPa (colors, in K), wind at 925 hPa (arrows, m s^{-1}) and Mean Sea Level Pressure (hPa, black contours), in ARCO-LR, CPLOA-LR and SSTHR-LR.

Figure S2. IOP16a, 26 Oct 2012 06UT: [*top panels*] Mean Sea Level Pressure (colors, in hPa), Radar reflectivities (green contours at 5, 20, and 100 mm h^{-1} equivalent) and CAPE over 1000 J kg^{-1} (red contour), and, [*bottom panels*] θ'_w at 925 hPa (color, in K) and wind at 925hPa (arrows, m.s^{-1}), in ARCO-LR, CPLOA-LR and SSTHR-LR.

Figure S3. IOP16a, 26 Oct 2012 12UT: Radar reflectivities (colors, in mm h^{-1} equivalent), Integrated Water Vapor over 32 kg m^{-2} (grey area), wind at 950 hPa (arrows, m s^{-1}) and CAPE over 1000 J kg^{-1} (red contour) in ARCO-SR, CPLOA-SR and SSTHR-SR.

For Peer Review

© 2017 Royal Meteorological Society

Figure S4. (a) Water budget components (mg m^{-2} s^{-1}) in CPLOA for IOP16a (26 October 2012, forecast basis: 26 October 00UTC]) for the low levels (0 - ∼500 m) [see the box in Fig. 10]. (b) Evaporation contribution (mg m^{-2} s^{-1}) to water budget for 26 October 2012 in ARCO, CPLOA, and SSTHR for SR forecast (forecast basis: 26 October 00UTC) and LR forecast (forecast basis: 25 October 00UTC).

Figure S5. IOP13 phase 3 (14-15 October 2012) at the LION buoy: [*top panels*] Time-series of 10m-wind speed (FF10, m s^{-1}), 2m-temperature (T2M, °C) and SST (°C) for ARCO (black), CPLOA (red) and SSTHR (blue) (forecast basis: 14 October 2012 00UT. Observations are the grey circles. [*bottom panel*] Time-serie of the ocean temperature (°C) profile simulated by CPLOA. The black line indicates the simulated MLD from a density criteria. The circles are observations from the bathymetric thermistance chain.

Figure S6. Same as Figure S5 but for IOP16a (26-27 October 2012) (forecast basis: 26 October 2012 00UT).

For Peer Review

© 2017 Royal Meteorological Society

References

Barnier B., Madec G., Penduff T., Molines J-M., Treguier A-M., Le Sommer J., Beckmann A., Biastoch A., Böning C., Dengg J., Derval C., Durand E., Gulev S., Rémy E., Talandier C., Theetten S., Maltrud M.E., McClean J., and De Cuevas B., 2006: Impact of partial steps and momentum advection schemes in a global ocean circulation model at eddy-permitting resolution. *Ocean Dyn.*, **56** (5-6), 543-567, doi:10.1007/s10236-006-0082-1.

Barthlott, C., S. Davolio, 2016: Mechanisms initiating heavy precipitation over Italy during HyMeX Special Observation Period 1: a numerical case study using to mesoscale models. *Quart. J. Roy. Meteorol. Soc.*, **142** (S1), 238-258, doi:10.1002/qj.2630.

Beuvier J., Sevault F., Herrmann M., Kontoyiannis H., Ludwig W., Rixen M., Stanev E., Béranger K., Somot S., 2010: Modeling the Mediterranean Sea interannual variability during 1961-2000: focus on the Eastern Mediterranean Transient. *J. Geophys. Res.*, **115**, C08517, doi:10.1029/2009JC005950.

Blanke, B., and P. Delecluse, 1993: Variability of the tropical Atlantic ocean simulated by a general circulation model with two different mixed layer physics, *J. Phys. Oceanogr*, **23**, 1363-1388.

Bouin, M-N., J-L. Redelsperger, C. Lebeaupin Brossier, 2017 (rev.): Processes leading to deep convection and sensitivity to sea-state representation during HyMeX IOP8 heavy precipitation event. *Quart. J. Roy. Meteorol. Soc.*

Bresson, E., Ducrocq V., Nuissier O., Ricard D., De Saint-Aubin C., 2012: Idealized numerical simulations of quasi-stationary convective systems over the Northwestern Mediterranean complex terrain. *Quart. J. Roy. Meteorol. Soc.*, **138**, 1751-1763, doi:10.1002/qj.1911.

Buzzi, A., Tartaglione N., Malguzzi P., 1998: Numerical Simulations of the 1994 Piedmont Flood: Role of Orography and Moist Processes. *Mon. Wea. Rev.*, **126** (9), 2369-2383.

Charnock, H., 1955: Wind stress over a water surface. *Quart. J. Roy. Meteor. Soc.*, **81**, 639-640.

Courtier, P., C. Freydier, J-F. Geleyn, F. Rabier, and M. Rochas, 1991: The ARPEGE project at Météo-France. *ECMWF workshop on numerical methods in atmospheric modeling*, **2**, 193-231.

Cuxart, J., P. Bougeault, and J-L. Redelsberger, 2000: A turbulence scheme allowing for mesoscale and large-eddy simulations. *Quart. J. Roy. Meteor. Soc.*, **126**, 1-30.

Davolio, S., Stocchi P., Benetazzo A., Bohm E., Riminucci F., Ravaioli M., Li X-M., Carniel S., 2015: Exceptional Bora outbreak in winter 2012: Validation and analysis of high-resolution atmospheric model simulations in the Northern Adriatic area. *Dyn. Atmos. Oc.*, **71**, 1-20.

Delrieu, G., Nicol J., Yates E., Kirstetter P-E., Creutin J. D., Anquetin S., Obled C., Saulnier G-M., Ducrocq V., Gaume E., Payrastre O., Andrieu H., Ayral P-A., Bouvier C., Neppel L., Livet M., Lang M., Parent-du-Châtelet J., Walpersdorf A., Wobrock W., 2005: The Catastrophic Flash-Flood Event of 8-9 September 2002 in the Gard Region, France: A First Case Study for the CévennesiVivarais Mediterranean Hydrometeorological Observatory. *J. Hydrometeorol.*, **6** (1), 34-52, doi:10.1175/JHM-400.1.

Donlon, C. J., M. Martin, J. Stark, J. Roberts-Jones, E. Fiedler, W. Wimmer, 2012: The operational sea surface temperature and sea ice analysis (OSTIA) system. *Remote Sens. Environ.*, **116**, 140-158.

Drobinski, P., Ducrocq V., Alpert P., Anagnostou E., Béranger K., Borga M., Braud I., Chanzy A., Davolio S., Delrieu G., Estournel C., Filali Boubrahmi N., Font J., Grubisic V., Gualdi S., Homar V., Ivancan-Picek B., Kottmeier C., Kotroni V., Lagouvardos K., Lionello P., Llasat M. C., Ludwig W., Lutoff C., Mariotti A., Richard E., Romero R., Rotunno R., Roussot O., Ruin I., Somot S., Taupier-Letage I., Tintoré J., Uijlenhoet R., Wernli H., 2014: HyMeX, a 10-year multidisciplinary program on the Mediterranean water cycle. *Bull. Amer. Meteorol. Soc.*, **95** (7), 1063-1082, doi:10.1175/BAMS-D-12-00242.1.

Ducrocq, V., D. Ricard, J-P. Lafore, F. Orain, 2002: Storm-scale numerical rainfall prediction for five precipitating events over France: On the importance of the initial humidity field, *Wea. and Forecast.*, **17**, 1236-1256.

Ducrocq, V., O. Nuissier, D. Ricard, C. Lebeaupin and T. Thouvenin, 2008: A numerical study of three catastrophic precipitating events over Southern France. II: Mesoscale triggering and stationarity factors. *Quart. J. R. Meteorol. Soc.*, **134**, 131-145.

Ducrocq V., Braud I., Davolio S., Ferretti R., Flamant C., Jansa A., Kalthoff N., Richard E., Taupier-Letage I., Ayral P.A., Belamari S., Berne A., Borga M., Boudevillain B., Bock O., Boichard J-L., Bouin M-N., Bousquet O., Bouvier C., Chiggiato J., Cimini D., Corsmeier U., Coppola L., Cocquerez P., Defer E., Delanoë J., Di Girolamo P., Doerenbecher A., Drobinski P., Dufournet Y., Fourrié N., Gourley J. J., Labatut L., Lambert D., Le Coz J., Marzano F.S., Molinié G., Montani A., Nord G., Nuret M., Ramage K., Rison B., Roussot O., Saïd F., Schwarzenboeck A., Testor P., Van Baelen J., Vincendon B., Aran M., Tamayo J., 2014: HyMeX-SOP1, the field campaign dedicated to heavy precipitation and flash flooding in the Northwestern Mediterranean. *Bull. Amer. Meteorol. Soc.*, **95** (7), 1083-1100, doi:10.1175/BAMS-D-12-00244.1.

Ducrocq, V., S. Davolio, R. Ferretti, C. Flamant, V. Homar Santaner, N. Kalthoff, E. Richard, H. Wernli, 2016: Advances in understanding and forecasting of heavy precipitation in Mediterranean through the HyMeX SOP1 field campaign. *Quart. J. R. Meteorol. Soc.*, **142** (S1), 1-6, doi:10.1002/qj.2856.

Duffourg, F., and V. Ducrocq, 2011: Origin of the moisture feeding the Heavy Precipitating systems over Southeastern France. *Nat. Hazards Earth Syst. Sci.*, **11**, 4, 1163-1178.

Duffourg, F., and V. Ducrocq, 2013: Assessment of the water supply to Mediterranean heavy precipitation: a method based on finely designed water budgets. *Atm. Sci. Lett.*, **14**, 133-138, doi:10.1002/asl2.429.

Duffourg, F., Nuissier O., Ducrocq V., Flamant C., Chazette P., Delanoë J., Doerenbecher A., Fourrié N., Di Girolamo P., Lac C., Legain D., Martinet M., Saïd F., Bock O., 2016: Offshore deep convection initiation and maintenance during HyMeX IOP16a. *Quart. J. Roy. Meteorol. Soc.*,

For Peer Review

142 (S1), 259-274, doi:1002/qj.2725.

Duffourg, F., K-O. Lee, V. Ducrocq, C. Flamant, P. Chazette, P. Di Girolamo, 2017 (rev): Role of moisture patterns in the backbuilding formation of HyMeX IOP13 Heavy Precipitaing Systems, *Quart. J. Roy. Meteorol. Soc.*.

Fairall C., Bradley E., Hare J., Grachev A., Edson J., 2003: Bulk parameterization of air-sea fluxes updates and verification for the coare algorithm. *J. Clim.*, **16**, 571-591.

Fouquart Y., Bonnel B., 1980: Computations of solar heating of the earths atmosphere: A new parameterization. *Beitr. Phys. Atmos.*, **53**, 35-62.

Fourrié, N., E. Bresson, M. Nuret, C. Jany, P. Brousseau, A. Doerenbecher, M. Kreitz, O. Nuissier, E. Sevault, H. Bénichou, M. Amodei, and F. Pouponneau, 2015: AROME-WMED, a real-time mesoscale model designed for HyMeX Special Observation Periods. *Geo. Model. Dev.*, **8**, 1919-1941, doi:10.5194/gmd-8-1919-2015.

Gaspar P., Grégoris Y., Lefevre J., 1990: A simple Eddy Kinetic Energy model for simulations of the oceanic vertical mixing: Tests at Station Papa and long-term upper ocean study site. *J. Geophys. Res.*, **95** (C9), 16179-16193.

Grifoll, M., J. Navarro, E. Pallares, L. Rafols, M. Espino, A. Palomares, 2016: Ocean-atmosphere-wave characterisation of a wind jet (Ebro shelf, NW Mediterranean Sea). *Nonlin. Processes Geophys.*, **23**, 143-158, doi:10.5194/npg-23-143-2016.

Homar, V., R. Romero, D. J. Stensrud, C. Ramis, and S. Alonso, 2003: Numerical diagnosis of a small, quasi-tropical cyclone over the western Mediterranean: Dynamical vs. boundary factors. *Q. J. R. Meteorol. Soc.*, **129**, 1469-1490.

Kain J. S., Fritsch J. M., 1990: A one-dimensional entraining/detraining plume model and its application in convective parameterization. *J. Atmos. Sci.*, **47** (23), 2784-2802.

Lafore, J-P., Stein J., Asencio N., Bougeault P., Ducrocq V., Duron J., Fischer C., Hreil P., Mascart P., Masson V., Pinty J-P., Redelsperger J-L., Richard E., Vila-Guerau de Arellano, J., 1998: The Meso-NH atmospheric simulation system. Part I: Adiabatic formulation and control simulations. Scientific objectives and experimental design. *Ann. Geophys.*, **16**, 90-109.

Lazar A., Madec G., Delecluse P., 1999: The deep interior downwelling, the Veronis effect, and mesoscale tracer transport parameterizations in an OGCM. *J. Phys. Ocean.*, **29** (11), 2945-2961.

Lebeaupin C., Ducrocq V., Giordani H., 2006: Sensitivity of torrential rain events to the sea surface temperature based on high-resolution numerical forecasts. *J. Geophys. Res.*, **111** (D12), 1-19, doi:10.1029/2005JD006541.

Lebeaupin Brossier, C., V. Ducrocq, and H. Giordani, 2008: Sensitivity of three Mediterranean heavy rain events to two different sea surface fluxes parameterizations in high-resolution numerical modeling. *J. Geophys. Res.*, **113**, D21109, doi:10.1029/2007JD009613.

Lebeaupin Brossier, C., Ducrocq V., Giordani H., 2009: Two-way one-dimensional high-resolution airsea coupled modelling applied to Mediterranean heavy rain events. *Quart. J. Roy. Meteorol. Soc.*, **135** (638), 187-204.

Lebeaupin Brossier C., Arsouze T., Béranger K., Bouin M-N., Bresson E., Ducrocq V., Giordani H., Nuret M., Rainaud R., Taupier-Letage I., 2014: Ocean Mixed Layer responses to intense meteorological events during HyMeX-SOP1 from a high-resolution ocean simulation. *Ocean Model.*, **84**, 84-103, doi:10.1016/j.ocemod.2014.09.009.

Lebeaupin Brossier, C., F. Léger, H. Giordani, J. Beuvier, M-N. Bouin, V. Ducrocq, N. Fourrié, 2017: Dense water formation in the north-western Mediterranean area during HyMeX-SOP2 in 1/36° ocean simulations: Ocean-atmosphere coupling impact. *J. Geophys. Res. Oceans*, **122**, doi:10.1002/2016JC012526.

Lellouche, J-M., O. Le Galloudec, M. Drévillon, C. Régnier, E. Greiner, G. Garric, N. Ferry, C. Desportes, C-E. Testut, C. Bricaud, R. Bourdallé-Badie, B. Tranchant, M. Benkiran, Y. Drillet, A. Daudin, C. De Nicola, 2013: Evaluation of global monitoring and forecasting systems at Mercator Océan. *Ocean Sci.*, **9**, *57-81*, doi:10.5194/os-9-57-2013.

Lyard F., Lefevre F., Letellier T., Francis O., 2006: Modelling the global ocean tides: modern insights from FES2004. *Ocean Dynamics*, **56** (5-6), 394-415.

Madec G., and the NEMO system team, 2008: NEMO ocean engine. *Note du Pole de modélisation, Institut Pierre-Simon Laplace (IPSL), France*, No 27 ISSN No 1288-1619.

Masson, V., 2000: A physically-based scheme for the urban energy budget in atmospheric models. *Bound.-Layer Meteor.*, **94**, 357-397.

Masson, V., P. Le Moigne, E. Martin, S. Faroux, A. Alias, R. Alkama, S. Belamari, A. Barbu, A. Boone, F. Bouyssel, P. Brousseau, E. Brun, J-C. Calvet, D. Carrer, B. Decharme, C. Delire, S. Donier, K. Essaouini, A-L. Gibelin, H. Giordani, F. Habets, M. Jidane, G. Kerdraon, E. Kourzeneva, M. Lafaysse, S. Lafont, C. Lebeaupin Brossier, A. Lemonsu, J-F. Mafhouf, P. Marguinaud, M. Mokhtari, S. Morin, G. Pigeon, R. Salgado, Y. Seity, F. Taillefer, G. Tanguy, P. Tulet, B. Vincendon, V. Vionnet, and A. Voldoire, 2013: The SURFEXv7.2 land and ocean surface platform for coupled or offline simulation of earth surface variables and fluxes. *Geosci. Model Dev.*, **6**, 929-960, doi:10.5194/gmd-6-929-2013.

Miglietta, M. M., A. Moscatello, D. Conte, G. Mannarini, G. Lacorata, R. Rotunno, 2011: Numerical analysis of a Mediterranean 'hurricane' over south-eastern Italy: Sensitivity experiments to sea surface temperature. *Atmos. Res.*, **101**, 412-426, doi:10.1016/j.atmosres.2011.04.006.

Millot, C., 1999: Circulation in the Western Mediterranean Sea. *J. Mar. Syst.*, **20** (1-4), 423-442.

Mlawer, E.J., S.J. Taubman, P.D. Brown, M.J. Iacono and S.A. Clough, 1997: Radiative transfer for inhomogeneous atmospheres: RRTM, a validated correlated-k model for the longwave. *J. Geophys. Res.*, **102**, 16663-16682.

Noilhan, J., and S. Planton, 1989: Simple parameterization of land surface processes for meteorological models. *Mon. Wea. Rev.*, **117**, 536-549.

Nuissier, O., V. Ducrocq, D. Ricard, C. Lebeaupin, S. Anquetin, 2008: A numerical study of three catastrophic precipitating events over southern France. I: Numerical framework and synoptic ingredients. *Quart. J. R. Meteorol. Soc.*, **134**, 111-130.

For Peer Review

© 2017 Royal Meteorological Society

Nuissier, O., Joly B., Joly A., Ducrocq V., Arbogast P., 2011: A statistical downscaling to identify the large-scale circulation patterns associated with heavy precipitation events over southern France. *Quart. J. R. Meteorol. Soc.*, **137**, 18121827, doi:10.1002/qj.866.

Pastor, F., M. J. Estrela, P. Penarrocha, and M. M. Millan, 2001: Torrential rains on the spanish Mediterranean coast: Modelling the effect of the sea surface temperature. *J. Appl. Meteorol.*, **40**, 1180 1195.

Pinty, J.-P., and P. Jabouille, 1998: A mixed-phased cloud parameterization for use in a mesoscale non-hydrostaticmodel: Simulations of a squall line and of orographic precipitation. Preprints, *Conf. on Cloud Physics*, Everett, WA, Amer. Meteor. Soc., 217-220.

Pullen J., Doyle J. D. , Signell R. P., 2006: Two-Way AirSea Coupling: A Study of the Adriatic. *Mon. Wea. Rev.*, **134**, 1465-1483, doi:10.1175/MWR3137.1.

Pullen J., Doyle J. D., Haack T., Dorman C., Signell R. P., Lee C. M.; 2007: Bora event variability and the role of air-sea feedback. *J. Geophys. Res.*, **112** (C3), 1-17, doi:10.1029/2006JC003726.

Rainaud, R., 2015: "*Modélisation couplée océan-atmosphère pour l'étude des évènements météorologiques intenses en Méditerranée occidentale*". PhD thesis. In french: *University Toulouse III, Paul Sabatier*, 218pp.

Rainaud, R., Lebeaupin Brossier C., Ducrocq V., Giordani H., Nuret M., Fourrié N., Bouin M-N., Taupier-Letage I., Legain D., 2016: Characterisation of air-sea exchanges over the Western Mediterranean Sea during the HyMeX SOP1 using the AROME-WMED model. *Quart. J. Roy. Meteorol. Soc.*, **142** (S1), 173-187, doi:10.1002/qj.2480.

Renault L., Chiggiato J., Warner J. C., Gomez M., Vizoso G., Tintore J., 2012: Coupled atmosphere-ocean-wave simulations of a storm event over the Gulf of Lion and Balearic Sea. *J. Geophys. Res.*, **117**, C09019, doi:10.1029/2012JC007924.

Ricard, D., Ducrocq V., Auger L., 2012: A climatology of the messcale environment associated with heavily precipitating avents over the Northwestern Mediterranean area. *J. Appl. Meteorol. Clim.*, **51**, 468-488.

Ricchi, A., M. M. Miglietta, P. P. Falco, A. Benetazzo, D. Bonaldo, A. Bergamasco, M. Sclavo, S. Carniel, 2016: On the use of a coupled ocean-atmosphere-wave model during an extreme cold air outbrerak over the Adriatic Sea. *Atmos. Res.*, **172-173**, 48-65, doi:10.1016/j.atmosres.2015.12.023.

Romero, R., Ramis C., Alonso S., Doswell C. A., Stenrud D. J., 1998: Mesoscale model simulations of three heavy precipitation events in the Western Mediterranean region. *Mon. Wea. Rev.*, **126** (7), 1859-1881.

Romero, R., C. Ramis, V. Homar, 2015: On the severe convective storm of 29 October 2013 in the Balearic Islands: observational and numerical study. *Quart. J. Roy. Meteorol. Soc.*, **141**, 1208-1222, doi:10.1002/qj.2429.

Roullet G., Madec G., 2000: Salt conservation, free surface, and varying levels: A new formulation for ocean general circulation models. *J. Geophys. Res.*, **105** (C10), 23927-23942, doi:10.1029/2000JC900089.

Seity Y., Brousseau P., Malardel S., Hello G., Bénard P., Bouttier F., Lac C., Masson V., 2011: The AROME-France Convective-Scale Operational Model. *Mon. Wea. Rev.*, **139**, 976-991.

Silvestro, F., Gabellani S., Giannoni F., Parodi A., Rebora N., Rudari R., Siccardi F., 2012: A hydrological analysis of the 4 november 2011 event in genoa. *Nat. Haz. Earth Sys. Sci.*, **12** (9), 2743-2752.

Small R., Campbell T., Teixeira J., Carniel S., Smith T., Dykes J., Chen S., Allard R., 2011: Air-sea interaction in the Ligurian Sea: Assessment of a Coupled Ocean-Atmosphere Model using in situ data from LASIE07. *Mon. Wea. Rev.*, **139** (6), 1785-1808, doi:10.1175/2010MWR3431.1.

Small R., Carniel S., Campbell T., Teixeira J., Allard R., 2012: The response of the Ligurian and Tyrrhenian Seas to a summer Mistral event: A coupled atmosphere-ocean approach. *Ocean Model.*, **48**, 30-44, doi:10.1016/j.ocemod.2012.02.003.

Stocchi, P. and Davolio, S., 2016: Intense air-sea exchanges and heavy rainfall: impact of the northern Adriatic SST. *Adv. Sci. Res.*, **13**, 7-12, doi:10.5194/asr-13-7-2016.

Taillefer, F., 2002: CANARI (Code for the Analysis Necessary for Arpege, for its Rejects and its Initialization): Technical documentation. *Technical report*, Groupe de Modélisation pour l'Assimilation et la Prévision, Centre National de Recherches Météorologiques, Météo-France, Toulouse, France. http://www.crnm.meteo.fr/gmapdoc/spip.php?article3.

Thévenot, O., M-N. Bouin, V. Ducrocq, C. Lebeaupin Brossier, O. Nuissier, J. Pianezze, F. Duffourg, 2016: Influence of the sea state on Mediterranean heavy precipitation: a case study from HyMeX SOP1. *Quart. J. Roy. Meteorol. Soc.*, **142** (S1), 377-389, doi:10.1002/qj.2660.

Valcke, S., 2013: The OASIS3 coupler: a European climate modelling community software. *Geosci. Model Dev.*, **6**, 373-388, doi:10.5194/gmd-6-373-2013.

Voldoire, A., B. Decharme, J. Pianezze, C. Lebeaupin Brossier, F. Sevault, L. Seyfried, V. Garnier, S. Bielli, S. Valcke, A. Alias, M. Accensi, F. Ardhuin, M-N. Bouin, V. Ducrocq, S. Faroux, H. Giordani, F. Léger, P. Marsaleix, R. Rainaud, J-L. Redelsperger, E. Richard, S. Riette, 2017: The seamless and multi-model coupling between atmosphere, land, hydrology, ocean, waves and sea-ice models based on SURFEX surface model using OASIS3-MCT. *Geosci. Model Dev. Disc.*, doi:10.5194/gmd-2017-91.

Warner, J. C., Armstrong B., He R., Zambon J. B., 2010: Development of a coupled ocean-atmosphere-wave-sediment transport (COAWST) modeling system. *Ocean Model.*, **35** (3), 230-244.

Xie S. P., Xu H. M. , Kessler W. S., Nonaka M., 2005: Air-sea interaction over the eastern pacific warm pool: Gap winds, thermocline dome, and atmospheric convection. *J. Clim.*, **18** (1), 5-20.

For Peer Review

© 2017 Royal Meteorological Society

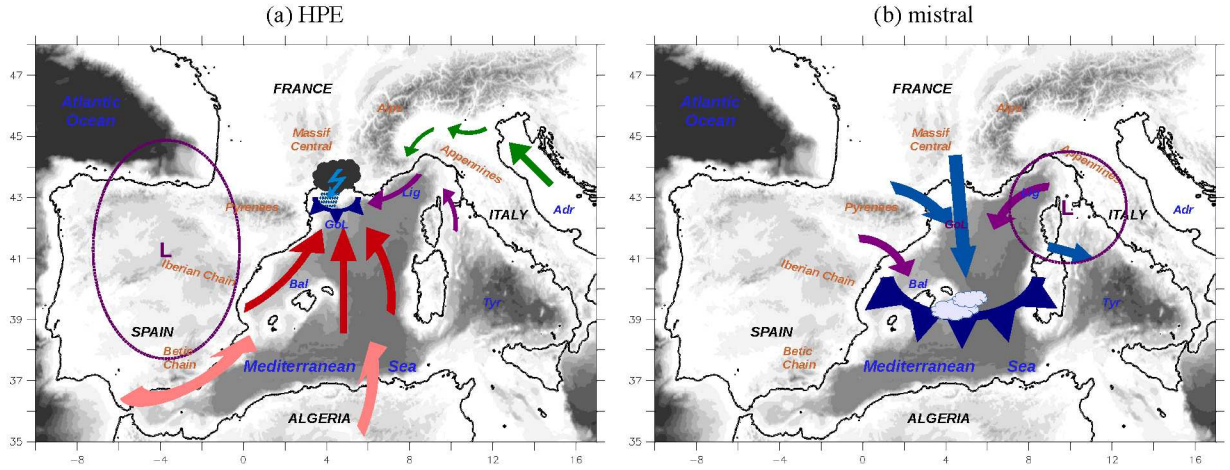


Figure 1. Schematic view of the low-level atmospheric circulation over the Western Mediterranean area: (a) during a HPE over South-Eastern France adapted from Ducrocq et al. (2016). The arrows represent the low-level circulation, the darkblue line with triangles represents the cold pool beneath the convective system. The location of the surface low pressure is indicated by the "L-ellipse"; (b) during a mistral/tramontane event. The location of the surface low pressure is indicated by the "L-ellipse". Convection often occur at the lee of the strong wind symbolized by a cold front represented by the darkblue line with triangles.

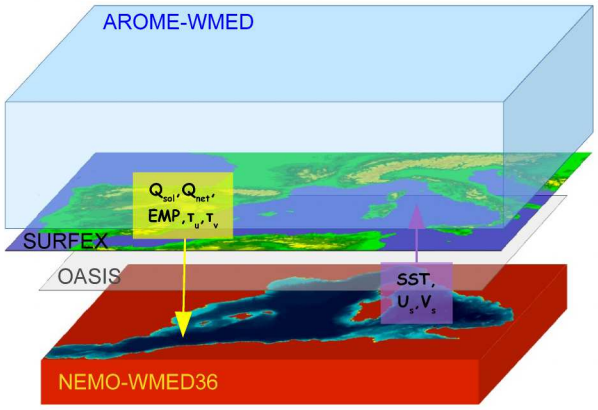


Figure 2. Architecture and domain of the AROME-NEMO WMED coupled system.

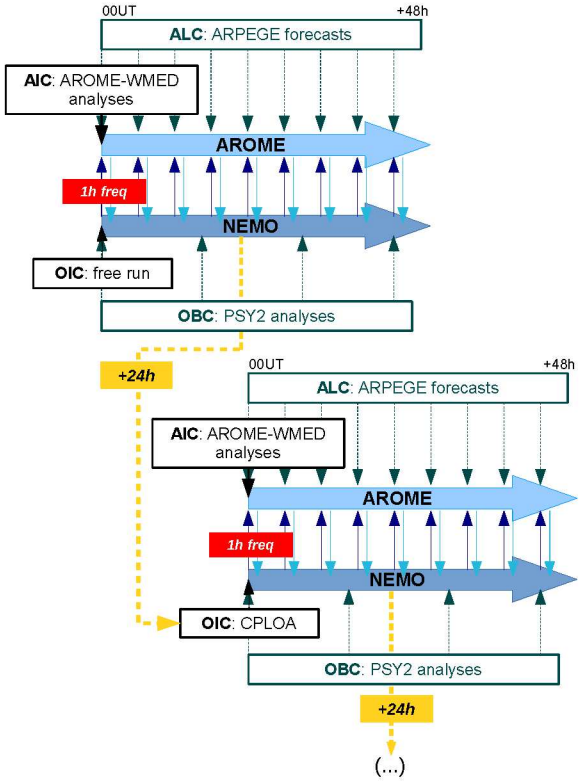


Figure 3. Numerical setup for the CPLOA experiment. ALC [OBC] stands for Atmospheric [Ocean] Lateral [Boundary] Conditions and AIC [OIC] for Atmospheric [Ocean] Initial Conditions.

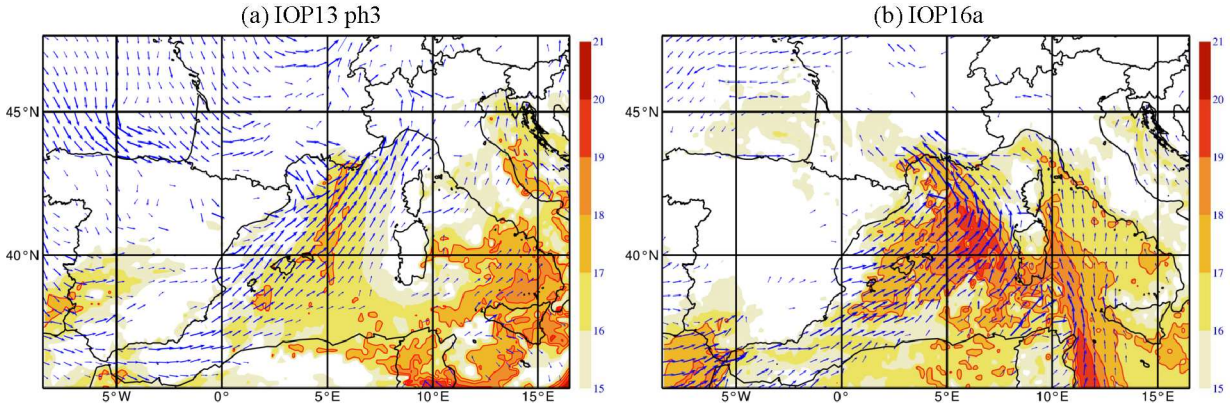


Figure 4. Wet-bulb temperature θ'_w (colors, in °C) and wind (arrows, above 5 m s^{-1}) at 950 hPa in AROME-WMED real-time forecasts: (a) for 14 September 2012 18UTC - IOP13 phase 3 (forecast basis: 14 September 2012 00UTC; range: +18h) and (b) for 26 September 2012 09UTC - IOP16a (forecast basis: 26 September 2012 00UTC; range: +9h). Source: http://hoc.sedoo.fr.

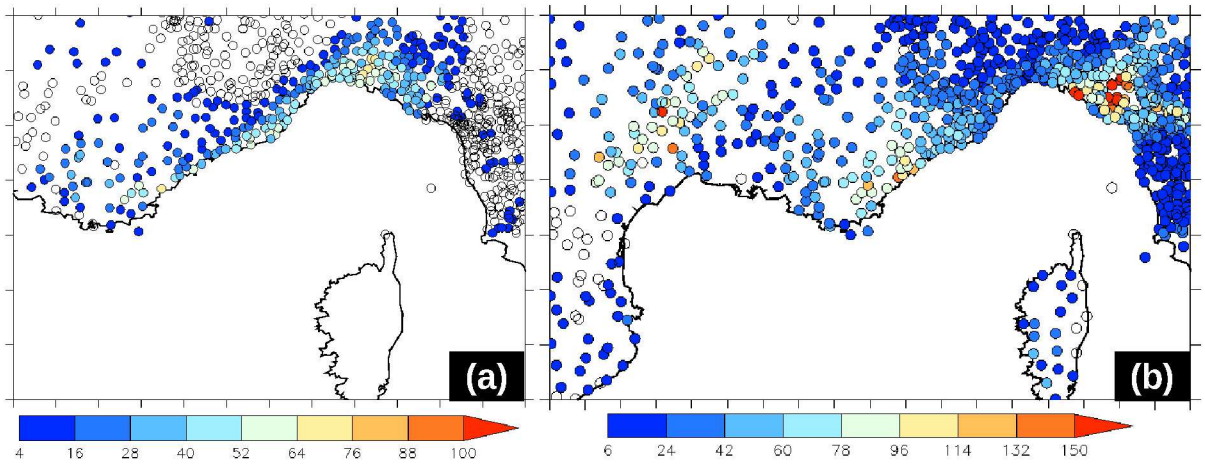


Figure 5. Daily-accumulated precipitation amounts (mm) from rain-gauges: (a) for 14 October 2012 (IOP13 phase 3) and (b) for 26 October 2012 (IOP16a).

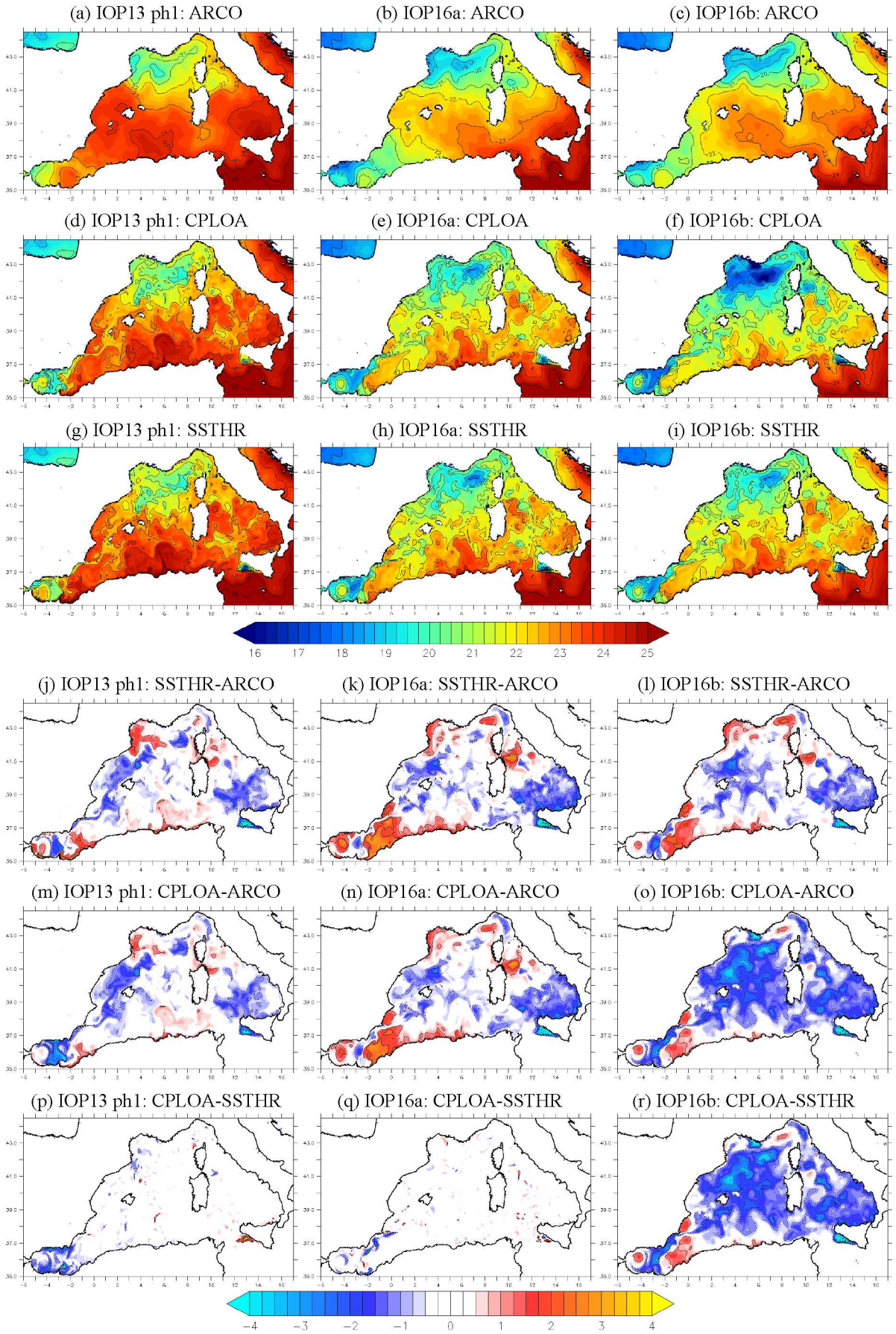


Figure 6. SST (°C) for 13 October 00UTC (IOP13 phase 1 - forecast basis: 11 October 2012; range: +48h) [*left panels*], for 27 October 00UTC (IOP16a - forecast basis: 25 October 2012; range: +48h) [*middle panels*] and for 29 October 00UTC (IOP16b - forecast basis: 27 October 2012; range: +48h) [*right panels*] for ARCO (a,b,c) CPLOA (d,e,f) and SSTHR (g,h,i) experiments. Differences in SST (°C): SSTHR minus ARCO (j,k,l); CPLOA minus ARCO (m,n,o) and CPLOA minus SSTHR (p,q,r) for 13 October 00UTC (IOP13 phase 1 - forecast basis: 11 October 2012; range: +48h) [*left panels*], for 27 October 00UTC (IOP16a - forecast basis: 25 October 2012; range: +48h) [*middle panels*] and for 29 October 00UTC (IOP16b - forecast basis: 27 October 2012; range: +48h) [*right panels*].

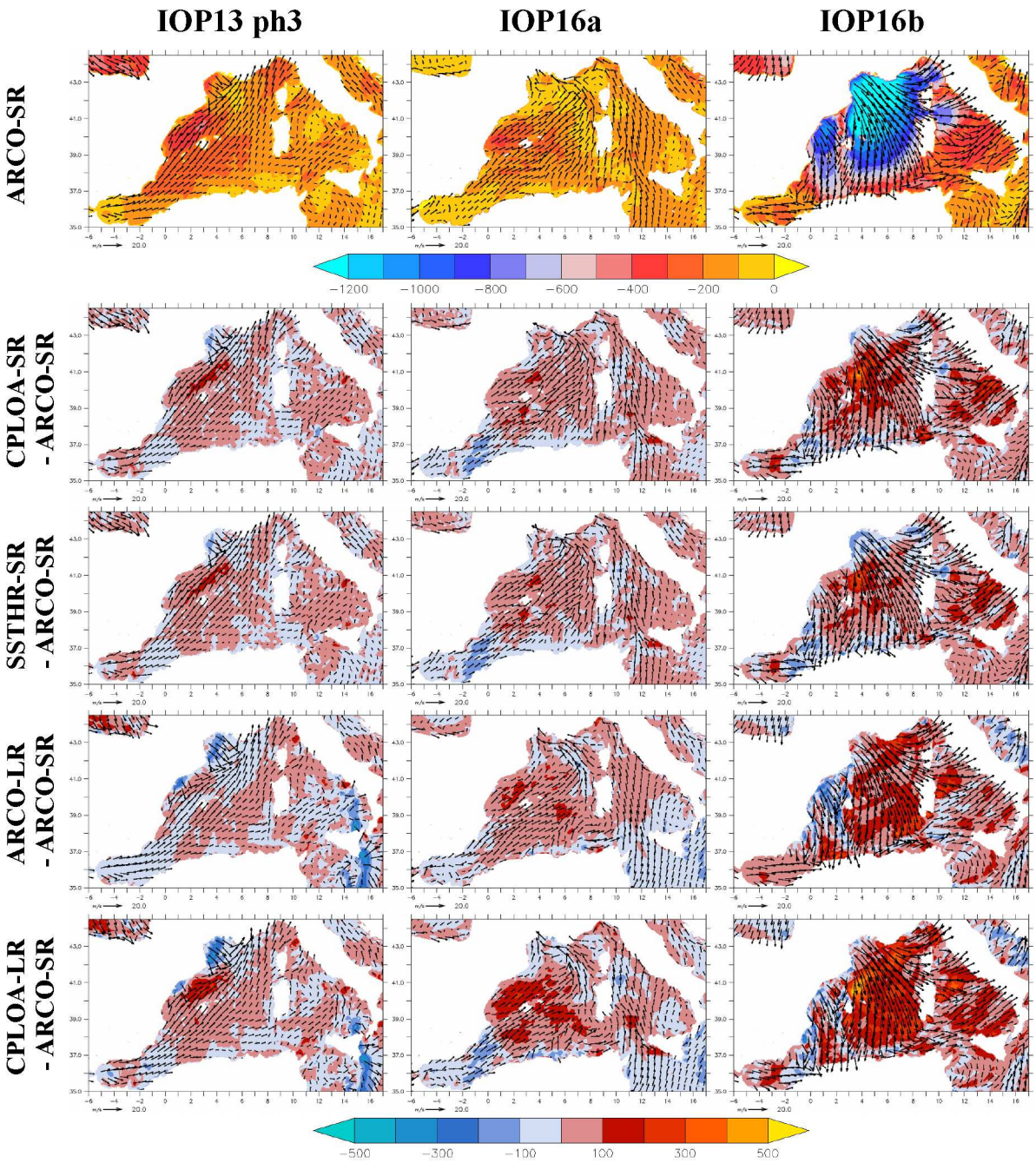


Figure 7. *First line*: Total turbulent heat flux (W m^{-2}) and wind (m s^{-1}) at first level of the AROME-WMED model (∼10 m-height) in ARCO-SR. Differences in total heat flux with ARCO-SR and forecast of the wind at first level for CPLOA-SR [*second line*], SSTHR-SR [*third line*], ARCO-LR [*fourth line*] and CPLOA-LR [*fifth line*]; for IOP13 phase 3 (14 October 18UTC) [*left*], IOP16a (26 October 12UTC) [*middle*] and IOP16b (28 October 00UTC) [*right*].

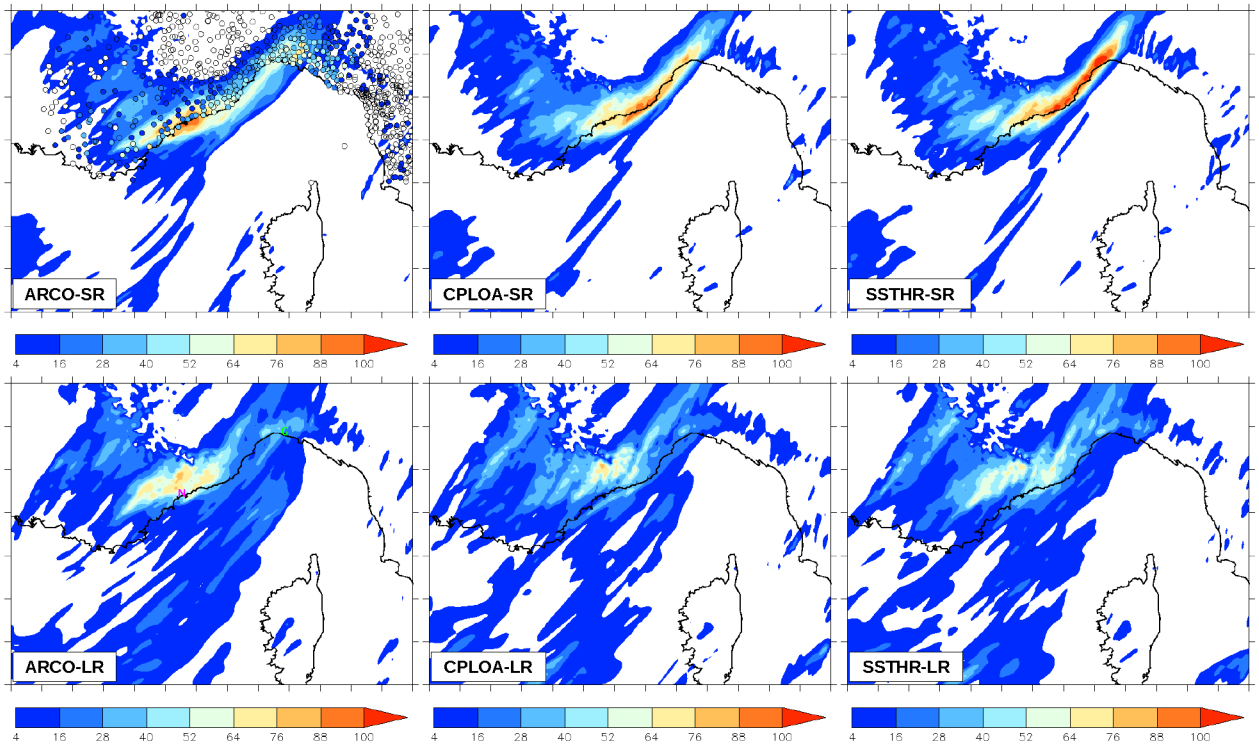


Figure 8. Accumulated rainfall (mm) from 14 October 16UTC to 15 October 00UTC (forecast basis: 14 October 2012 00UT [*top panels*] and 13 October 2012 00UT [*bottom panels*]) for ARCO [*left*], CPLOA [*middle*] and SSTHR [*right*] experiments. In the upper left panel, the colored circles correspond to the daily-accumulated precipitation amounts (mm) for 14 October 2012 from rain-gauges (See also Fig. 5a). In the lower left panels, the purple "N" indicates Nice location; the green "G" indicates Genoa location.

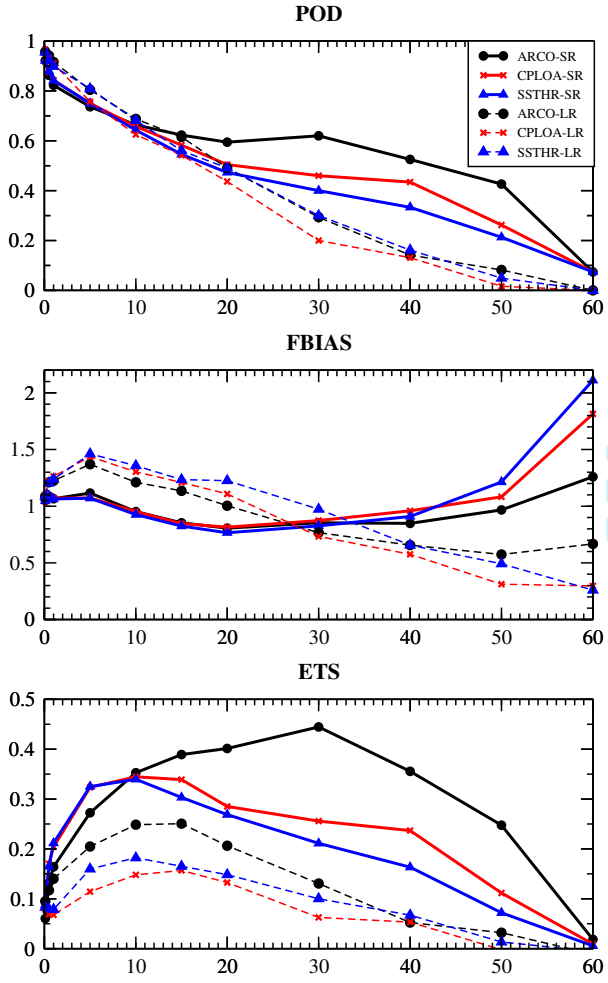


Figure 9. Probability of detection (POD), frequency bias (FBIAS) and equitable threat score (ETS) as a function of a considered threshold for the 24h-accumulated rainfall (mm) from 14 October 00UTC to 15 October 00UTC (forecast basis: 14 October 2012 00UT for SR experiments and 13 October 2012 00UT for LR experiments). A perfect forecast has FBIAS, POD and ETS equal to 1.

For Review

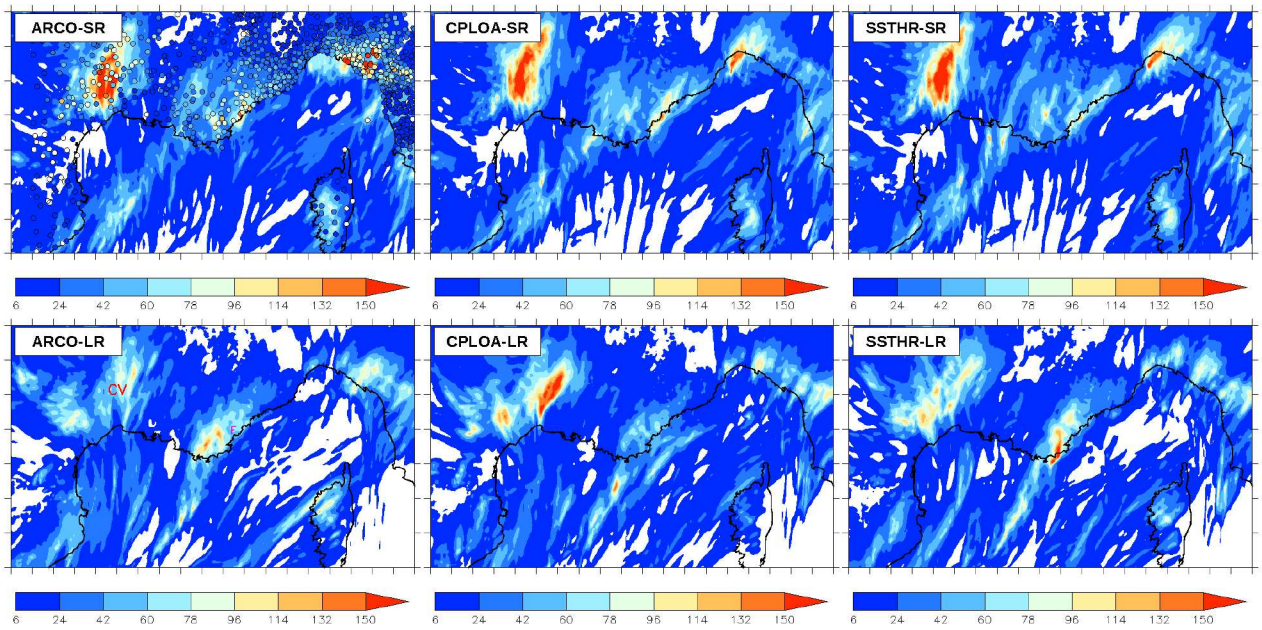


Figure 10. Accumulated rainfall (mm) from 26 October 00UTC to 27 October 00UTC (forecast basis: 26 October 2012 00UT [*top panels*] and 25 October 2012 00UT [*bottom panels*]) for ARCO [*left*], CPLOA [*middle*] and SSTHR [*right*] experiments. In the upper left panel, the colored circles correspond to the daily-accumulated precipitation amounts (mm) for 26 October 2012 from rain-gauges (See also Fig. 5b). In the lower left panels, the purple "F" indicates Frejus (Var) location; the red "CV" indicates the Cévennes area.

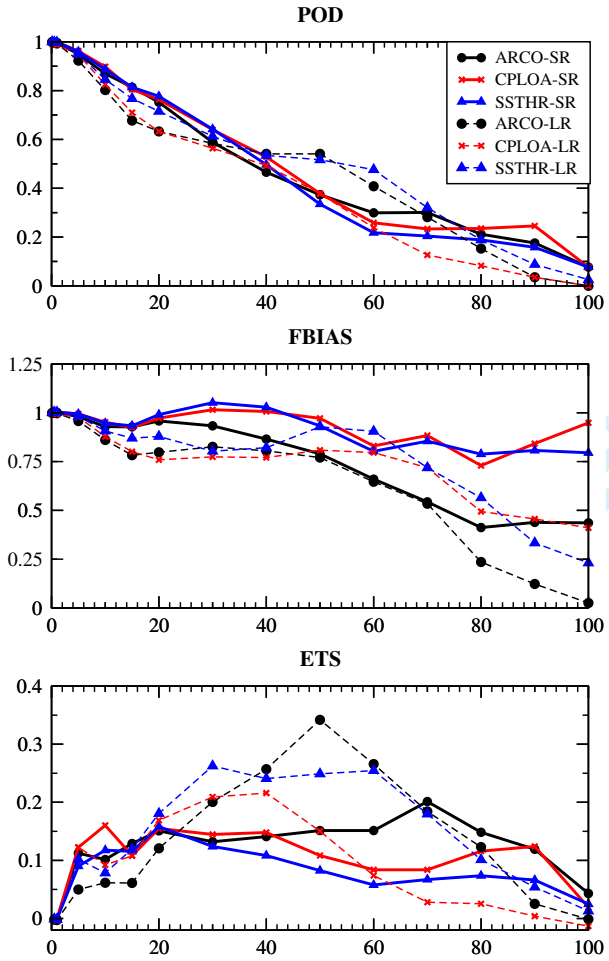


Figure 11. As Fig. 9 but considering the 24h-accumulated rainfall (mm) from 26 October 00UTC to 27 October 00UTC (forecast basis: 26 October 2012 00UT for SR experiments and 25 October 2012 00UT for LR experiments).

For Review

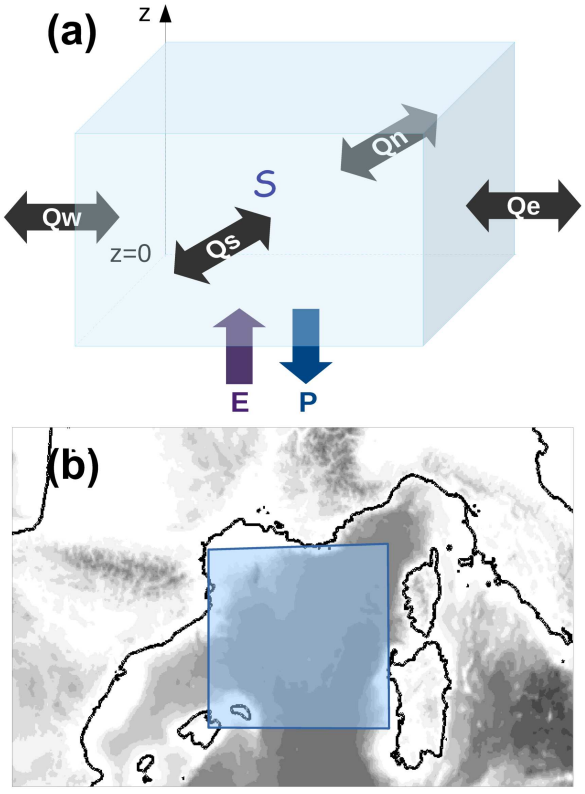


Figure 12. (a) Scheme of the water content budget and components: S is the storage of total atmospheric water within the budget box, E is the surface evaporation, P precipitation and Qn, Qe, Qs, Qw are the vertically integrated horizontal fluxes of water through the four sides of the box. (b) Budget box location.

For Review

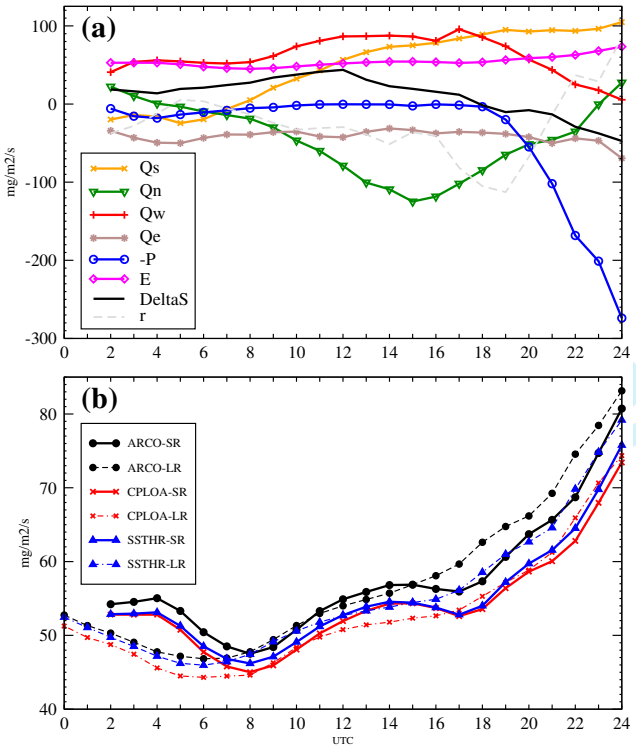


Figure 13. (a) Water budget components (mg m^{-2} s^{-1}) in CPLOA for IOP13 phase 3 (14 October 2012, forecast basis: 14 October 00UTC]) for the low levels (0 - ∼500 m) [see the box in Fig. 12]. (b) Evaporation contribution (mg m^{-2} s^{-1}) to water budget for 14 October 2012 in ARCO, CPLOA, and SSTHR for SR forecast (forecast basis: 14 October 00UTC) and LR forecast (forecast basis: 13 October 00UTC).

For Review

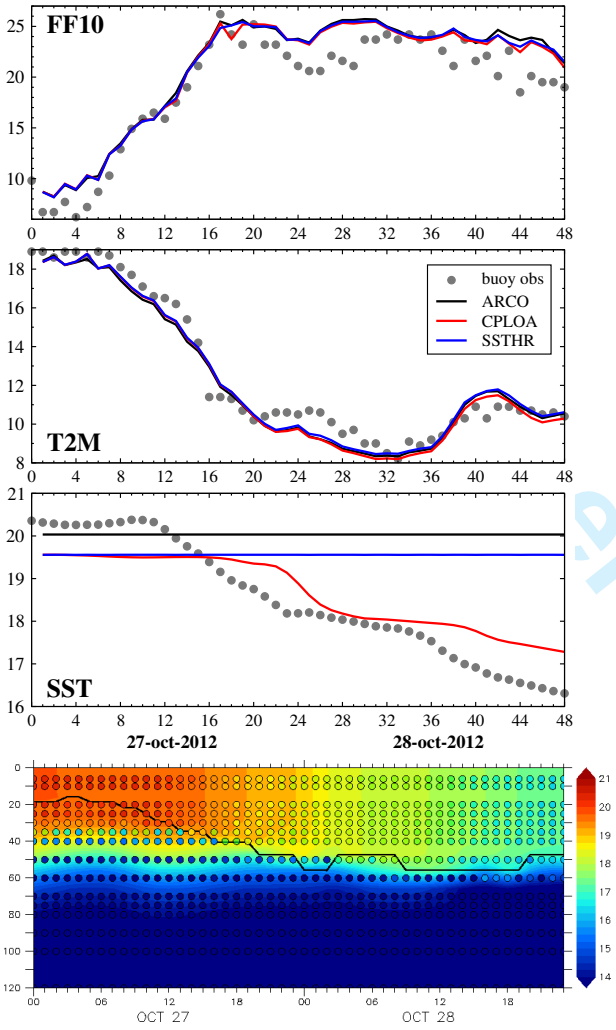


Figure 14. IOP16b (27-28 October 2012) at the LION buoy: [*top panels*] Time-series of 10m-wind speed (FF10, m s^{-1}), 2m-temperature (T2M, °C) and SST (°C) for ARCO (black), CPLOA (red) and SSTHR (blue) (forecast basis: 27 October 2012 00UT. Observations are the grey circles. [*bottom panel*] Time-serie of the ocean temperature (°C) profile simulated by CPLOA. The black line indicates the simulated MLD from a density criterion. The circles are observations from the bathymetric thermistance chain.

er Review

Table 1. Bias (mm), Root Mean Squared Error (RMSE, mm) and correlation (CORR) for the simulated 24h-cumulated rainfall amounts on 14 October 2012 against raingauge observations.

	SR		
	ARCO	CPLOA	SSTHR
BIAS	-0.426	0.018	0.537
RMSE	14.235	16.394	18.646
CORR	0.662	0.586	0.538
	LR		
	ARCO	CPLOA	SSTHR
BIAS	0.719	0.862	1.768
RMSE	16.934	18.461	18.306
CORR	0.464	0.321	0.365

Table 2. As Table 1 but for the simulated 24h-cumulated rainfall amounts on 26 October 2012.

	SR		
	ARCO	CPLOA	SSTHR
BIAS	-4.967	-1.760	-1.648
RMSE	29.872	33.688	34.610
CORR	0.450	0.334	0.291
	LR		
	ARCO	CPLOA	SSTHR
BIAS	-8.864	-7.614	-6.271
RMSE	26.435	31.860	28.444
CORR	0.590	0.400	0.500

Table A. Schematic 2×2 contingency table for the definition of scores, given a threshold thr for the rainfall amount.

	simulation $< thr$	simulation $\geq thr$
observation $< thr$	a	b
observation $\geq thr$	c	d

For Peer Review